Elsevier Editorial System(tm) for Fuel
Manuscript Draft

Manuscript Number: JFUE-D-16-02322R2

Title: Characterisation of DME-HCCI combustion cycles for formaldehyde and hydroxyl UV-vis absorption

Article Type: Research paper

Keywords: HCCI; low-temperature combustion; dimethyl ether combustion; UV-vis light absorption; formaldehyde; OH

Corresponding Author: Dr. Ulugbek Azimov, PhD

Corresponding Author's Institution: University of Northumbria

First Author: Ulugbek Azimov, PhD

Order of Authors: Ulugbek Azimov, PhD; Nearchos Stylianidis, MSc; Nobuyuki Kawahara, PhD; Eiji Tomita, PhD

Abstract: We investigated time-resolved ultraviolet-visible (UV-vis) light absorbance to identify the formation behaviour of formaldehyde (HCHO) and hydroxyl (OH) within the wavelength range of 280-400 nm in a homogeneous charge compression ignition (HCCI) engine fuelled with dimethyl ether (DME). The time-resolved HCHO and OH profiles at different initial pressures showed that HCHO absorbance increased in the low-temperature reaction (LTR) and thermal-ignition preparation (TIP) regions and decreased gradually as the combustion approached the high-temperature reaction (HTR) region. At higher intake pressures, HCHO absorbance decreased and OH absorbance increased. The time-resolved absorbance spectra of HCHO, with peaks at 316, 328, 340, and 354 nm for all combustion cycles, were evaluated and it was found that average absorption at 328 nm was slightly higher than at 316, 340, and 354 nm. For knocking combustion cycles, the absorbance of HCHO in the LTR region was high for cycles with low knock intensity and low for cycles with high knock intensity, showing a high level of OH absorbance. Chemical kinetics analyses showed that for different fuel/oxidiser ratios, initial O2 concentration and intake temperature had no effect on in-cylinder temperatures in the LTR or TIP regions. However, they did have significant effects on HTR combustion. In-cylinder temperature in the LTR region had less effect on HCHO and H2O2 formation than pressure.

- HCHO absorbance increased in LTR and TIP regions and decreased in HTR region
- HCHO decreased as RoHR increased and *vice versa*
- O_2 and intake temperature did not affect in-cylinder temperature in LTR and TIP
- O_2 and intake temperature had significant effects on HTR combustion
- HCHO concentration was very low when knock intensity was very high, and *vice versa*

Abstract

We investigated time-resolved ultraviolet-visible (UV-vis) light absorbance to identify the formation behaviour of formaldehyde (HCHO) and hydroxyl (OH) within the wavelength range of 280–400 nm in a homogeneous charge compression ignition (HCCI) engine fuelled with dimethyl ether (DME). The time-resolved HCHO and OH profiles at different initial pressures showed that HCHO absorbance increased in the low-temperature reaction (LTR) and thermal-ignition preparation (TIP) regions and decreased gradually as the combustion approached the high-temperature reaction (HTR) region. At higher intake pressures, HCHO absorbance decreased and OH absorbance increased. The time-resolved absorbance spectra of HCHO, with peaks at 316, 328, 340, and 354 nm for all combustion cycles, were evaluated and it was found that average absorption at 328 nm was slightly higher than at 316, 340, and 354 nm. For knocking combustion cycles, the absorbance of HCHO in the LTR region was high for cycles with low knock intensity and low for cycles with high knock intensity, showing a high level of OH absorbance. Chemical kinetics analyses showed that for different fuel/oxidiser ratios, initial O_2 concentration and intake temperature had no effect on in-cylinder temperatures in the LTR or TIP regions. However, they did have significant effects on HTR combustion. In-cylinder temperature in the LTR region had less effect on HCHO and H_2O_2 formation than pressure.

Key words: HCCI, low-temperature combustion, dimethyl ether combustion, UV-vis light absorption, formaldehyde, OH

Nomenclature

DME	dimethyl ether
HCCI	homogeneous charge compression ignition
DARS	digital analysis of reactive systems
RCM	rapid compression machine
CAD	crank angle degree
TDC	top dead centre
BDC	bottom dead centre
IVC	intake valve closure
LTC	low-temperature combustion
LTR	low-temperature reaction
NTC	negative temperature coefficient
TIP	thermal ignition preparation
HTR	high-temperature reaction
$ROHR_{max}$	maximum rate of heat release (J/deg)
$ROHR_{LTR\ peak}$	peak of heat release rate in low-temperature reaction region (J/deg)
KI	knock intensity (MPa)
P_{in}	intake pressure (MPa)
P_{EC}	end-of-compression pressure (MPa)
T_{in}	intake temperature (K)
HCHO	formaldehyde
OH	hydroxyl
ICCD	intensified charge-coupled device

1. Introduction

Homogeneous charge compression ignition (HCCI) engines have drawn the attention of many researchers due to their high efficiency and lower nitrogen oxide (NOx) and particulate matter (PM) emissions. Most recent studies on HCCI have focussed on four-stroke engines [1, 2]. Dimethyl ether (DME: CH_3OCH_3) is an attractive alternative to conventional diesel fuel for compression-ignition (CI) engines because it auto-ignites favourably and burns with little soot formation [3, 4]. DME is an oxygenated hydrocarbon, with a low carbon-to-hydrogen ratio and the absence of a C-C bond, leading to very low emissions of PM during combustion. DME is also considered a promising alternative fuel with the potential to solve air-pollution problems

caused by NOx emissions [4]. DME shows very strong low-temperature kinetic reactions in HCCI. The processes of low-temperature reactions (LTRs) involve branched chain reactions, the evolution of which is determined by the processes of parallel and consecutive elementary reactions, with the participation of free radicals and atoms. It is known that slow combustion of hydrocarbons follows a degenerate branched mechanism and is characterised by a large variety of elementary reactions, with the participation of free radicals having complex structures. Apparently, these specific features are responsible for the kinetic manifestations of the oxidation processes: the slow combustion of hydrocarbons, shown by cool flames and a negative temperature coefficient (NTC) of the reaction rate, collectively called the LTR region, the thermal-ignition preparation (TIP), the high-temperature reaction (HTR), and thermokinetic oscillations (Fig. 1). Interest in the cool flames, NTCs, and oscillations is high because of the need to take into account the influence of these factors on the dynamics, kinetics, and mechanisms of hydrocarbon oxidation and combustion in practice. Thus, a study of an HCCI engine fuelled with DME may provide useful information on the low-temperature kinetic reactions for HCCI operation with other fuels. The oxidation of DME has been examined in several studies and research has led to the development of detailed and reduced chemical kinetics models of DME combustion [5-11].

To understand the DME oxidation mechanism in an HCCI engine, an experimental kinetic study of DME combustion is needed. An effective way to study DME combustion is to use a spectrum analysis to determine the major active aldehyde group species, such as formaldehyde (HCHO) and other active radicals [12, 13]. Studies have examined HCHO absorption in a constant volume vessel or a reactor [14, 15]. A few studies have also examined HCHO formation and absorption under normal engine conditions [16, 17]. HCHO is an important intermediate species that influences the low-temperature chain reactions in hydrocarbon, oxygenated, and biofuel combustion processes [18, 19]. Some research groups have stated that, under certain experimental conditions, HCHO can act as a hydroxyl (OH) radical inhibitor and can suppress engine knock [20, 21]. Other groups have emphasised that HCHO reacts as a promoter of

auto-ignition by advancing auto-ignition timing, resulting in a higher heat release rate [22]. Thus, it is important to detect *in situ* and monitor HCHO formation inside the engine cylinder [23-27] to understand in detail the in-cylinder processes and be able to design advanced combustion control systems [28]. Existing diagnostic methods for HCHO detection are based mostly on the laser-induced fluorescence (LIF) technique [23, 29, 30]. Previous attempts by other groups to measure HCHO absorption in the infrared (IR) region [31-34] were successful; however, it was concluded that it would be almost impossible to readily detect and measure HCHO concentrations due to a lack of sensitivity and/or interference from other molecules as combustion products, such as H_2O, CO_2, and CO [35, 36]. Understanding the HCHO formation process would help to resolve problems related to knocking combustion. In internal combustion (IC) engines, engine knock is related to HCHO in the hot spots (exothermic centres) of the slow oxidation process prior to autoignition [37, 38]. HCHO is an important intermediate species in the cool flames preceding the main combustion. It has been shown that the local HCHO concentration decreases dramatically in locations with peak heat release rates [39].

Thus, the objective of this study was to investigate the combustion characteristics in an HCCI engine fuelled with DME. Ultraviolet-visible (UV-vis) absorption spectroscopy was used to determine the light absorption of chemical species during the DME combustion process, which includes low-temperature oxidation and high-temperature ignition. The major aim was to characterise the combustion cycles in terms of time-resolved spectra of HCHO and OH species, as representative indicators of low-temperature oxidation and thermal ignition, respectively, during HCCI combustion. Chemical kinetics analyses were performed to evaluate the effects of pressure and temperature on HCHO and OH formation, taking into account the interactions of these species with H_2O_2 and HO_2. The absorbances of HCHO and OH during knocking combustion in HCCI were investigated by estimating the knock intensity derived from in-cylinder pressure oscillations.

2. Experimental setup and procedure

Test engine and light absorbance acquisition system

An HCCI fuelled with DME was studied in an optical compression-expansion test engine with a single cylinder and a compression ratio of 9.0. Figure 2 shows a schematic diagram of the test engine with its specification and experimental conditions summarised in Table 1. The engine crank was driven externally by a 2,000-W induction motor and made to rotate at a fixed rpm. The DME was premixed with gas at a ratio of 20% oxygen to 80% argon (Ar) at molar proportions equivalent to ϕ = 0.30. Argon was used instead of nitrogen, to increase the in-cylinder temperature at the end of compression by decreasing the heat capacity of the in-cylinder gas-fuel mixture, and to initiate HCCI combustion at a compression ratio that was significantly lower than those usually used in conventional HCCI engines. The DME-O_2-Ar fuel mixture was supplied to the mixture tank, where it was heated to the required temperature and maintained at the required pressure. During operation, the intake valve remained open, and the fuel mixture was sucked into the cylinder and pushed back into the mixture tank. When the thermocouple reading had stabilised, the intake valve was closed at around bottom dead centre (BDC), and the fuel mixture was compressed, autoignited, and combusted. Changes in the gas pressure were measured using a Kistler 6052B pressure transducer during the compression and expansion strokes. The compressed gas temperature range accessible in the compression-expansion test engine was relevant to combustion in HCCI and related engines, but the in-cylinder pressure at top dead centre (TDC) was somewhat lower because the initial pressure was less than 1 atmosphere. Thus, good temporal resolution was more readily achieved, but at the expense of longer ignition delays than those encountered in practical applications. The volumetric heat release in the final stage of ignition was also lower as a result of the reduced gas densities. However, pressure oscillations were still observed, even with very lean mixtures. The gaseous charge admitted to the cylinder of the compression-expansion test engine was premixed at the molecular level. Thus, unlike engines with a normal induction system for evaporating liquid fuels, the problem of distinguishing the effect of the initial spatial composition variations from the spatial temperature field variations did not arise.

UV-vis absorption measurements were performed using a specially designed cylinder head, equipped with sapphire windows, optical fibres, a deuterium lamp, and an Andor Shamrock-163 spectrograph with an attached intensified charge-coupled device (ICCD; Fig. 3). Data were acquired, stored, and processed using the Andor Solis software.

The UV-vis and infrared spectral absorbances were determined by applying the Beer-Lambert law to the measured spectral transmission:

$$A(\lambda) = \log_{10}\left[\frac{I_0(\lambda)}{I(\lambda)}\right] = \varepsilon c L \quad (1),$$

where $A(\lambda)$ is the spectral absorbance, $I_0(\lambda)$ is the intensity through air, $I(\lambda)$ is the intensity through a DME-O_2-Ar mixture, and ε, c, and L are the molar absorption coefficient, molar concentration, and measurement length, respectively. For HCHO and OH UV-vis light absorption experiments, a deuterium lamp was used as the light source. A deuterium lamp is a low-pressure gas-discharge light source often used in spectroscopy when a continuous spectrum in the UV region is needed. The arc created in the lamp excites the molecular deuterium contained within the bulb to a higher energy state. The deuterium then emits light as it transitions back to its initial state. The light is then transmitted to the combustion chamber through an optical fibre with a collimator and further transmitted from the combustion chamber through a 12-point optical fibre with a collimator, and finally to the spectrometer (SR-163; Andor Technology), which was equipped with an ICCD (DK720-18F-04; Andor Technology) (Fig. 3). Spectral absorbance measurements were made under engine conditions for HCHO and OH in the region of 280–400 nm.

3. Results and discussion

3.1 Time-resolved UV-vis HCHO and OH absorbance spectra

UV-vis light absorbance was investigated to identify the formation behaviour of HCHO and OH during HCCI combustion. Light absorbance spectra were obtained for 10 selected piston positions. The crank-angle resolution for the spectral results was 11 crank-angle degrees (CAD;

~3 ms at 600 rpm). Two molecular species were apparent in the spectra. The absorption was caused by HCHO at wavelengths of 316, 328, 340, and 354 nm, and by OH at a wavelength of 308 nm. Figure 4 shows the absorbance spectra at different intake pressures and temperatures. Figure 4 (A), (B), (C) and (D) show the time-resolved absorbance spectra at the pre-set initial temperatures and pressures at different ICCD exposure start times. Figure 4 (E), (F), (G) and (H) show ROHR obtained for the same initial conditions as the absorbance data was taken. For these results the absorbance and in-cylinder pressure were obtained concurrently. The purpose for showing this graph was to demonstrate the consistent trend in HCHO and OH peaks which occur at the specified wavelengths for a number of experimental conditions. It is seen that as the time between the start of LTR and the start of HTR decreases the HCHO peaks gradually become weaker and OH peaks become more distinct. This suggests that there is a correlation between the residence of LTR+TIP regions and HCHO formation. It can be seen that the intensity of the spikes at 316, 328, 340, and 354 nm changed due to the formation of HCHO [40, 41] and the absorption at those wavelengths was consistent for all of the combustion cycles.

It was found that average absorption at 328 nm was slightly higher than at 316, 340, and 354 nm. The significance of this observation was to find out at which wavelength the absorption level was the highest in order to focus on this particular wavelength band in the future and use the type of laser with a narrow bandwidth. From 340 CAD, which corresponds to TIP, to 370 CAD, which in turn corresponds to a gradual decrease in in-cylinder pressure during the expansion stroke, the intensities of the spikes at 316, 328, 340, and 354 nm changed due to an increase in OH concentration at 308 nm, due to H_2O_2 decomposition. Previous investigations have reported different timings for the H_2O_2 decrease and OH increase. Westbrook [42] reported that the H_2O_2 decrease and the OH increase took place almost simultaneously, and H_2O_2 decomposition was the initiator of thermal ignition. However, Kuwahara and Ando [43] reported that the H_2O_2 decrease started earlier than the OH increase, and they showed that the rapid OH increase started during the final stage of the H_2O_2 decrease. Nevertheless, both research groups concurred that the OH rapid increase occurred in the TIP region. In our case the combustion progresses under

HCCI conditions, which, by nature, is not really homogeneous and we suspect that during the compression stroke there are different states of mixture and local equivalence ratio distribution in the cylinder which can affect the states of cool and hot chemistry. Even if we try to completely eliminate any in-cylinder turbulence effects in HCCI combustion, we must accept that it will be practically impossible. Therefore, we believe that it was important to demonstrate HCHO and OH trends experimentally. Nevertheless, to support the statement made above we can say that there is an overlap for HCHO and OH formation as shown in Figure 4 (C) and (D). This may be due to various reasons and require further investigation that may be done in the future studies.

Figure 5 shows the trends of time-resolved HCHO and OH absorbance peaks versus the maximum rate of heat release (ROHR) at various inlet temperatures and pressures. As can be seen, the peak absorbance of HCHO decreased as the maximum rate of heat released in the HTR region increased. We observed a consistent trend for all HCHO absorption wavelengths. In contrast, the peak absorbance of OH increased with the increase in heat release in the HTR region. This confirmed the trend that the peak amount of HCHO formed in the LTR and TIP regions affected the high-temperature combustion reactions and we can make assumptions based on the results in figure 5 where we can see the trend of absorbance vs max peak of ROHR that occurs in HTR region. It shows clear positive trend for OH vs ROHRmax and negative trend for HCHO vs ROHRmax. This suggests that HCHO may act as an inhibitor of the chain-branching reactions in the TIP regions before HTRs occur. This statement can be made based on the knowledge of chemistry that occurs in the low-temperature reaction region where H_2O_2 decomposes to OH or in reverse, and HCHO reacts with OH producing HCO and water. It is basically a competition between H_2O_2 and HCHO formation developed based on the species concentration and reaction rate. The trend in figure 5 suggests that HCHO decreases and OH increases as ROHR increases and vice versa, so we anticipate the effect of formaldehyde suppressing chain-branching reactions and holding OH formation before HTR reactions occur. Figure 5 shows the absorbance results for the range of pressures and temperatures, that's why pressure was not indicated on this figure.

This is consistent with the results of other studies showing that the temperature before the LTR does not contribute to the progress of reactions in the low-temperature combustion region, and that formation of HCHO inhibits HTRs [44]. This correlation has shown the general and opposite trends for HCHO and OH vs ROHRmax and supports our statements made throughout this manuscript. The purpose was to demonstrate the correlation of HCHO and OH absorption with the energy release.

Time-resolved absorption was studied at intake absolute pressures of 50, 60, and 85 kPa. Figures 6 and 7 show that at 50 and 60 kPa, the peak absorbance of HCHO from 340 CAD increased gradually as the start of ICCD exposure changed further for different cycles and there was no visible increase in OH. For cycles at 85 kPa intake pressure (Fig. 8), HCHO absorbance was almost not seen as the start of ICCD exposure changed further from 340 CAD, but OH absorbance increased significantly at 308 nm. The equivalence ratio for all three conditions was maintained at 0.3. These results suggest that, at lower intake pressures, reactions in LTR and TIP prevail and HCHO is formed as the piston moves from BDC to TDC. At higher intake pressures, the combustion passes the LTR temperature threshold more quickly and progresses to the HTR region, where the decomposition of H_2O_2 permits access to secondary reactions and forms very reactive OH radicals [45]. Previous studies showed that at higher intake valve closing pressures of 225kPa, H_2O_2 concentration increases during the $H_2O_2(+M) = OH + OH(+M)$ reaction [46]. This is because at higher pressures the high concentration of the mixture leads to a sufficient concentration of HO_2, which is less reactive than other free radicals, forming H_2O_2.

3.2 Effect of intake pressure on HCHO and OH absorbance

We studied the effects of intake pressure on HCHO and OH absorbance in DME-HCCI combustion experiments. The fuel equivalence ratio and temperature were set constant, at 0.3 and 293, respectively, and the mixture pressure in the mixture tank (Fig. 2) was varied from 48 to 85 kPa. The exposure start was fixed at TDC (360 CAD) and 5 CAD after TDC (365 CAD), with an exposure duration of 11 CAD; hundreds of individual combustion cycles were recorded.

The absorbance obtained for each interval of 11CAD is the average of that exposure duration. Therefore, we believe that no allowance was needed with the variation of temperature and pressure during compression. Figure 9 shows the absorbance results at selected initial pressures in order to investigate the effect of pressure; therefore, the pressure was indicated on the graph. The pressures relate to the pressure in the mixture tank or intake pressure. This figure shows that HCHO absorbance that was taken at TDC (360 CAD), increased in the thermal ignition preparation region when the ROHR was very low. In contrast, when the ROHR in the HTR region was high, HCHO absorbance was minimal but OH absorbance increased significantly. Due to the combustion cyclic variations, the effects of intake pressure on HCHO and OH absorbance remain unclear. However, the general trend in Figure 10, where the absorbance was taken at TDC (360 CAD) and 5 CAD after TDC (365 CAD), shows that with an increase in OH absorbance, HCHO absorbance decreased.

We also compared the HCHO and OH average absorbance levels at different wavelengths for nearly 120 individual combustion cycles and found that the HCHO absorbance at 328 nm was slightly higher than that at other wavelengths. Figure 11 shows that at lower intake pressures, the OH absorbance level at 308 nm was lower than the HCHO absorbance level but for higher intake pressures, OH absorbance was significantly higher than HCHO absorbance.

The effect of in-cylinder pressure on the amount of heat released in the LTR region, and any correlation with the HCHO and OH absorbance, was unclear. Thus, to investigate these trends – and the effects of in-cylinder pressure and temperature on HCHO and OH formation during DME fuel compression ignition – chemical kinetics analyses of DME-O_2-Ar and DME-O_2-N_2 mixture combustion were performed. First, a single-zone HCCI model was used to compare various DME detail and reduced mechanisms for in-cylinder pressure with that from experiments. The DME chemical kinetics mechanisms considered for this comparison were DME 2000 [8], DME 2008 [9], the DME skeletal mechanism [10], and the San Diego mechanism (http://combustion.ucsd.edu). The intake valve closing (IVC) time was 180° CA BTDC and the simulation ran for 360° CA. The mixture pressure and temperature at IVC were set as in these

experiments. The base San Diego mechanism with a DME sub-mechanism showed the closest match with the experiments and was selected for further chemical kinetics analyses in Digital Analysis of Reactive Systems (DARS) software with Rapid Compression Machine (RCM) model [47]. This mechanism takes into account recent chemical-kinetic studies of DME combustion processes [11]. The DME sub-mechanism included 14 new reactions that involved five new species (CH_3OCH_3, CH_3OCH_2, $CH_3OCH_2O_2$, $CH_2OCHOOH$, and HO_2CH_2OCHO). The mechanism was developed and validated by comparison with experimental results and different chemical kinetics mechanisms over a wide range of temperatures, pressures, and equivalence ratios [9, 48-51]. In the reaction $HO_2CH_2OCHO \leftrightarrow OH + CH_2O + CO_2 + H$, the decomposition of hydroperoxymethyl formate releases an additional OH radical and forms CH_2O, H, and CO_2.

The DARS-RCM model that includes Woschni heat transfer model was used to study the effects of pressure, temperature, and initial fuel and oxidant concentrations on HCHO and OH formation. DME-RCM combustion conditions were evaluated at intake temperatures of 293, 303, 313, 323, and 450 K, end-of-compression pressures of 20, 50, 80, and 100 bars, and the initial fuel-oxidiser mass fractions shown in Table 2. Initial fuel-oxidiser mass fractions were chosen based on: Case 1 (A) – Eq. ratio 0.3, Case 2 (B) - Eq. ratio 0.6 and Case 3 (C) – Eq. ratio 1.0. The sum of mass fractions (DME + O2 + (Ar or N2)) for each case was equal to 1. The initial temperature was 293 K and pressure at the end of compression was 100 bar. The equivalence ratio wasn't mentioned there to avoid the readers' confusion when they may think that if the equivalence ratio increases then HTR region temperature should also increase. We want to draw the attention that with the increase of fuel concentration, O_2 concentration wasn't fixed but decreased. The objectives of this study were to show whether thermal or chemical effects are more important for the combustion progress in the HTR region. This analysis was used to investigate the combined effects of the fuel concentration, oxidant, in-cylinder temperatures and pressure on HCHO, H_2O_2, and OH formation in the LTR, TIP, and HTR regions during DME-HCCI combustion.

Figure 12 shows conditions (A), (B), and (C) with different DME/O_2 and O_2/Ar ratios, based on the initial mass fractions shown in Table 2. The in-cylinder temperature level at which LTR and TIP reactions occurred (the pink region on Figure 12, T = 800 ÷ 1,000 K) remained the same for all conditions as the DME/O_2 ratio increased. The HCHO concentration also increased with the increase in pressure in the LTR and TIP regions, as highlighted. As the O_2/Ar ratio increased, the in-cylinder temperature, ROHR, and OH concentration increased in the HTR region. From this, we can conclude that the O_2 concentration does not affect the temperature change in the LTR or TIP regions and does not affect HCHO or H_2O_2 formation; however, it plays an important role in the HTRs. These results also suggest that the temperature in the low-temperature region did not have any effect on high-temperature combustion and OH formation before the HTR reactions have been suppressed by the increased amount of HCHO. This chemical kinetics study was introduced as an extension to the experiments to study these effects.

Previous work on DME chemical kinetics analysis in a constant volume chamber, by Kuwahara et al. [43], proposed a four-stage oxidation process of a hydrocarbon fuel with a cool flame. The transition from cool flame to NTC was determined by the competition between O_2 addition reactions and OH subtraction reactions, accompanied by the formation of HCHO. Major products of the cool flame and NTC regimes were oxygen-containing species like HCHO and H_2O_2. Based on these results, it can be presumed that the highest radical activity in the LTR region was associated with the chemistry that occurs when the HCHO concentration increased. This caused a subsequent deceleration in the rate of pressure rise, leading to low or negligible chain branching and a fall in the overall heat release, because OH radicals were replaced as a propagating species, mainly by less reactive HO_2 radicals. The maximum deceleration of the pressure rise rate corresponded to the reaction taking place at its minimum rate in the negative temperature-dependent regime. The evolution of the thermal ignition and the subsequent acceleration in the pressure rise rate can be attributed predominately to the production and decomposition of H_2O_2.

At lower initial temperatures, it was observed that the HCHO formed in the LTR and TIP regions had a greater effect on HTR combustion than in-cylinder temperature. This can be stated based on the chemical kinetics analysis results shown in Figure 12. All three conditions (A), (B) and (C) were simulated with the same initial temperature T=293K and the pressure at the end of compression, P=100 bar. We can see from this figure that the combustion in LTR and TIP regions for conditions (A), (B) and (C) occurs in the same temperature range (pink layer). However, the concentration of HCHO that is formed during LTR and TIP regions increases as DME/O2 ratio increases, although O2/Ar ratio decreases. Fuel concentration is correlated with the amount of HCHO and its concentration increases from (A) towards (C), and on the contrary, the in-cylinder temperature and ROHR in the HTR region decreases. Figure 12 shows that in the case of a lower temperature (T_{in} = 293 K), when Ar was used as the dilutant gas, the HCHO concentration in LTR and TIP regions increased commensurate with an increase in the DME/O_2 ratio; this inhibited the high combustion rate, so the temperature in the HTR region decreased despite the increase in fuel concentration. All arguments here are about trying to find out whether it is the effect of temperature during LTR and TIP region or the effect of HCHO on temperature increase in HTR and if both then which one has a greater influence. For all cases, rapid OH growth was observed after the HCHO concentration dropped. HCHO increased as the initial fuel concentration increased. As the O_2/Ar ratio decreased, the in-cylinder temperature and OH also decreased. As expected, the initial O_2 concentration in the mixture directly affected the combustion intensity and the in-cylinder temperature in the HTR region; however, it did not affect the in-cylinder temperature in the LTR or TIP regions (the pink region on Figure 13, T = 800 ÷1,000 K). In contrast, when the initial temperature was high (T_{in} = 450 K), as shown in Figure 13(A) for Ar gas, despite the decrease in the O_2/Ar ratio, the combustion rate in the HTR region was extremely high. However, the heat release in the cool flame and NTC regions was negligibly small. Therefore, based on the results of chemical kinetics analysis shown in Figure 12 (A), (C) and Figure 13 (A), (B) we have compared two cases with different initial temperatures, 293K and 450K, with the same DME/O2 and O2/Ar ratios. If we look at the region

where LTR and TIP occur we can find that the temperature range in these regions for both cases (293K and 450K) is almost the same. However, the temperature and ROHR in HTR region are higher for the case with 450K. We believe that this is a very important finding because it can suggest that in the real HCCI engine how to implement the combustion control. On the one hand, we want to control HCHO and its effect on OH and on the other, we want to control HTR region where the power is mainly generated. This is especially important when the fuel reactivity controlled combustion concepts are developed.

When N_2 was used as a dilutant gas, as shown in Figure 13(B), due to the higher heat capacity of N_2 versus Ar, the resulting in-cylinder combustion temperature in the HTR region was much lower and heat release in the cool flame and NTC regions was seen distinctly. Thus, comparing these two different temperature cases, we can presume that the intake temperature does not affect the in-cylinder temperature level in the LTR or TIP region. These results demonstrate the validity of the experiments when Ar was used instead of N_2 as a dilutant gas. The results of the chemical kinetics analysis with Ar and N_2 show that for both conditions the LTR and TIP occur at almost the same temperature range meaning that there is no effect of temperature in these regions on HTR combustion (temperature range in LTR+TIP regions for Ar and N_2 cases are the same). However, the temperature and ROHR in HTR region are very much lower in the case with N_2 background gas. If this is the case, we can presume that only HCHO formed in these low-temperature regions can have an effect on HTR combustion. Comparing (A)-(C) and (B)-(D) in the Figure 13 we can see that the concentration of HCHO in the LTR+TIP region is almost doubled in N_2-case compared to that of Ar-case. The computation has validated the fact that the temperature ranges in the LTR+TIP region, when Ar and N_2 background gases were used, are the same. However, for N_2 the HCHO concentration is increasing and suppressing the OH formation and therefore the amount heat release in HTR region.

To study the effects of pressure on HCHO formation, we compared two different conditions: 1) the initial temperature was kept constant and in-cylinder pressure was varied, and 2) the in-cylinder pressure was kept constant and the initial temperature was varied. Figure 14 shows

the comparison of these conditions. The change in cylinder pressure had a greater effect on the amount of HCHO formed than the change in initial temperature. However, the intake temperature had a greater effect on the ignition delay than pressure. At fixed pressure and higher intake temperatures, the ignition delay advances, HCHO is formed earlier, and the combustion rate increases; however, the concentration of HCHO formed in the LTR and TIP regions decreases. These combined effects of temperature, pressure, initial fuel concentration, and O_2 concentration suggest that the increased HCHO concentration at higher in-cylinder pressures is due to a larger amount of air/fuel charge in the cylinder, while the lower in-cylinder temperature is due to the decreasing O_2 concentration in the mixture, and the lower HCHO concentration at higher initial temperatures is due to the evolution of the thermal ignition. The subsequent acceleration in the pressure rise rate can be attributed predominately to the production and decomposition of H_2O_2, and to the competition between O_2 addition reactions and OH subtraction reactions, accompanied by the formation of HCHO.

3.3 Time-resolved UV-vis HCHO and OH absorbance spectra for knocking combustion

The formation of HCHO and OH species, and their lifetimes in the LTR, NTC, and TIP regions, provides better understanding of knocking combustion mechanism and helps us to control knocking in HCCI engines. We studied the effect of HCHO formed in the LTR and TIP regions on the rate of combustion and engine knock. A fixed exposure duration of 11 CAD with various ICCD-triggered instances was applied to each cycle. On the left, Figures 15–19 show the combustion cycles with different in-cylinder pressure oscillations and knock intensities. On the right, they show HCHO and OH absorbances detected at different crank angles. The maximum amplitude of the high-frequency component of the pressure (2.5–12 kHz) was taken as the knocking intensity of the corresponding cycle by applying a fast Fourier transform (FFT) to the pressure signal.

Figure 15 shows the absorption scan in the LTR region; we observed very small peaks of HCHO during combustion with moderate knock intensities. Figure 16 shows an almost

negligible level of knock intensity and a high level of HCHO absorbance. This suggests that the reaction rate was such that it produced high concentration of HCHO in the LTR and TIP regions and thus failed to result in knock in the HTR region. Figures 17 and 18 show the correlation between the high concentration of OH, the low concentration of HCHO, and combustion with high knock intensity. In Figure 19, with the exposure start time at 375 CAD after TDC, it can be seen that the OH concentration decreased. The HCHO concentration is always low when the OH concentration is high.

The results in Figures 15–19 show a clear trend between knock intensity and HCHO/OH formation. This work helps to characterise combustion cycles with HCHO and OH absorption during combustion in a DME-HCCI engine. These results will help in understanding the complex processes of intermediate species formation during combustion, and in the design of advanced optical sensors for effective combustion control.

4. Conclusions

From this study, the following conclusions can be drawn:

1. The time-resolved HCHO and OH profiles during the DME-O_2-Ar mixture combustion cycles showed that the HCHO absorbance increased in the LTR and TIP regions and decreased gradually as combustion approached the HTR region. The opposite trend was observed for OH absorbance profiles. OH was at a minimum in the LTR region and increased as the combustion approached the HTR region. The increased HCHO concentration at higher in-cylinder pressures is due to a larger amount of air/fuel charge in the cylinder. The lower in-cylinder temperature is due to the reduced O_2 concentration in the mixture.

2. Due to the existing combustion cyclic variability, it was difficult to precisely determine, from the experiments, the effect of pressure on HCHO and OH formation in the LTC; thus, a chemical kinetics analysis was performed. The chemical kinetics analysis showed that the initial O_2 concentration and intake temperatures did not affect the in-cylinder temperature in the LTR or TIP regions. However, they had significant effects on HTR combustion. At an intake temperature

of 450 K, with Ar as the dilutant gas, the rate of heat release was extremely high. The ROHR in the cool flame and NTC regions did not change. When N_2 was used as the dilutant gas, a distinct ROHR in the cool flame and NTC regions was observed.

3. A correlation between the in-cylinder spectral HCHO/OH formation and knocking intensity was observed. By applying different ICCD exposure timing vs. crank angle degree settings, it was possible to demonstrate a trend whereby HCHO concentration was very low and OH concentration was very high when knock intensity was very high, and *vice versa*.

The English in this document has been checked by at least two professional editors, both native speakers of English. For a certificate, please see:
http://www.textcheck.com/certificate/miOQ24

References

[1] Flowers DL, Killingsworth NJ, Espinosa-Loza F, Martinez-Frias J, Aceves SM, Krstic M, Dibble R. Demonstrating Optimum HCCI Combustion with Advanced Control Technology. SAE Paper 2009-01-1885; 2009.

[2] Manente V, Zander C, Johansson B, Tunesta P, Cannella W. An advanced internal combustion engine concept for low emissions and high efficiency from idle to max load using gasoline partially premixed combustion. SAE Paper 2010-01-2198; 2010.

[3] Semelsberger TA, Borup RL, Greene HL. Dimethyl ether (DME) as an alternative fuel. J Power Sources 2006;156:497-511

[4] Arcoumanis C, Bae C, Crookes R, Kinoshita E. The potential of di-methyl ether (DME) as an alternative fuel for compression-ignition engines: a review. Fuel 87;2008:1014-30.

[5] Curran HJ, Fisher SL, Dryer FL. The reaction kinetics of dimethyl ether. II: low-temperature oxidation in flow reactors. Int J Chem Kinetics 2000;32(12):741-59.

[6] Dagaut P, Boettner JC, Cathonnet M. Chemical kinetic study of dimethyl ether oxidation in a jet stirred reactor from 1 to 10 atm: experiments and kinetic modeling. Proc Comb Inst 1996;26:627-32.

[7] Kim H, Cho S, Min K. Reduced chemical kinetic model of DME for HCCI combustion. SAE Paper 2003-01-1822; 2003.

[8] Kaiser EW, Wallington TJ, Hurley MD, Platz J, Curran HJ, Pitz WJ and Westbrook CK. Experimental and modeling study of premixed atmospheric-pressure Dimethyl Ether-air flames. J Phys Chem 2000;35: 8194-8206

[9] Zhao Zh, Chaos M, Kazakov A and Dryer FL. Thermal decomposition reaction and a comprehensive kinetic model of dimethyl ether. Int J Chem Kinet 2008;40:1-18.

[10] Bhagatwala A, Luo Z, Lu TF, Shen H, Sutton JA, Lu T, Chen JH. Numerical and

experimental investigation of turbulent DME jet flames. Proc Combust Inst 2015;35:1157-1166.

[11] Prince JC, Williams FA. A short mechanism for the combustion of dimethyl-ether. Comb Flame 2015;162:3589-3595.

[12] Iida N. Combustion analysis of methanol-fueled active thermo-atmosphere combustion (ATAC) engine using a spectroscopic observation. SAE Paper 940684; 1984.

[13] Hultqvist A, Cristensen M, Johansson B, Richter M, Alden M. A study of the homogeneous charge compression ignition combustion process by chemiluminescence imaging. SAE Paper 1999-01-3680; 1999.

[14] Mackey MW, Daily JW, McKinnon JT, Riedel EP. High-temperature UV-visible absorption spectral measurements and estimated primary photodissociation rates of formaldehyde, chlorobenzene and 1-chloronaphthalene. J Photochem Ptotobiol A: Chemistry 1997;105:1-6.

[15] Bai X, Metz T, Ossler F, Alden M, Absorption of formaldehyde (H_2CO) in the A1A2<--X1A1 band system at elevated temperatures and pressures. Spectrochimica Acta 2004;(A 60):821-28.

[16] Withrow L, Rassweiler GM. Formaldehyde formation by preflame reactions in an engine spectroscopic study. Indust Eng Chemistry 1934;26(12):1256-62.

[17] Iijima A, Yoshida K, Shoji H. A study of autoignition in an HCCI engine by using light absorption and emission spectroscopy in: Proceedings of the 7th International Symposium COMODIA 2008: 297-303.

[18] Klein R and Schoen LJ. Role of formaldehyde in combustion. Chapter in Advances in Chemistry 1958;20:58-68.

[19] Lewis B and von Elbe G. Combustion Flames and Explosions of Gases, 1987, 3rd edition, ISBN:97801244675141987.

[20] Sarner G, Richter M, Alden M, Hildingsson L. Simultaneous PLIF measurements for visualisation of formaldehyde- and fuel- distributions in a DI HCCI engine. SAE Paper 2005-01-3869; 2005.

[21] Yao M, Zheng Z, Liu H. Progress and recent trends in homogeneous charge compression ignition (HCCI) engines. Prog Energy Comb Sci 2009;35:398-437.

[22] Kim SK, Ito K, Yoshihara D, Wakisaka T. Application of a genetic algorithm to the optimization of rate constants in chemical kinetic models for combustion simulations of HCCI engines. JSME Int J 2005;48:717-724.

[23] Brackmann C, Nygren J, Bai X, Li Z, Bladh H, Axelsson B, Denbratt I, Koopmans L, Bengston P, Alden M. laser-induced fluorescence of formaldehyde in combustion using third harmonic Nd:YAG laser excitation. Spectrochimica Acta 2003;59:3347-3356.

[24] Kim T and Ghandhi JB. Investigation of light load HCCI combustion using formaldehyde planar laser-induced fluorescence. Proc Comb Inst 2005;30:2675-2682.

[25] Donkerbroek AJ, van Vliet AP, Somers LMT, Frijters PJM, Klein-Douwel RJH, Dam HJ, Meerts WL, ter Meulen JJ. Time-and space-resolved quantitative LIF measurements of formaldehyde in a heavy-duty diesel engine. Combust Flame 2010;157, 155-166.

[26] Ehn A, Johansson O, Bood J, Arvidsson A, Li B, Alden M. Fluorescence lifetime imaging in a flame. Proc Combust Inst 2011;33:807-813.

[27] Azimov U, Kawahara N, Tomita E. UV-visible light absorption by hydroxyl and formaldehyde and knocking combustion in a DME-HCCI engine. Fuel 2012;98:164-175.

[28] Docquier N, Candel S. Combustion control and sensors; a review. Prog Energy Comb Sci 2002;28:107-150.

[29] Merchant SS, Goldsmith CF, Vandeputte AG, Burke MP, Klippenstein SJ, Green WH. Understanding low-temperature first-stage ignition delay: Propane. Combust Flame 2015;162:3658-3673.

[30] Burkert A and Paa W. Ignition delay times of single kerosene droplets based on formaldehyde LIF detection. Fuel 2016;167:271-279.

[31] Staak M, Gash EW, Venables DS, Ruth AA. The rotationally-resolved absorption spectrum of formaldehyde from 6547 to 6804 cm-1. J Mol Spectroscopy 2005;229:115-121.

[32] Zhao W, Gao X, Deng L, Huang T, Wu T, Zhang W. Absorption spectroscopy of formaldehyde at 1.573μm. J Quant Spectroscopy Radiat Trans 2007;107:331-339.

[33] Morajkar P, Schoemaecker C, Fittschen C. Absolute absorption cross sections for two selected lines of formaldehyde around 6625 cm-1. J Mol Specrtroscopy 2012;281:18-23.

[34] Wang S, Davidson DF, Hanson RK. High-temperature laser absorption diagnostics for CH2O and CH3CHO and their application to shock tube kinetic studies. Combust Flame 2013;160:1930-1938.

[35] Burkert A, Triebel W, Stafast H, Konig J. Single-shot imaging of gas temperatures in low-temperature combustion based on laser-induced fluorescence of formaldehyde. Proc Combust Inst 2002;29:2645-2651.

[36] Zhang F, Shuai S, Wang Z, Zhang X, Wang J. A detailed oxidation mechanism for the prediction of formaldehyde emission from methanol-gasoline SI engines. Proc Combust Inst 2011;33:3151-3158.

[37] Bauerle B, Behrendt F, Warnatz J. Detection of hot spots in the end gas of an internal combustion engine using two-dimensional LIF of formaldehyde. in: Proc of the 25th International Symposium on Combustion, Combust Inst 1994:135-41.

[38] Graf N, Gronki J, Schultz C, Baritaud T, Cherel J, Duret P, Lavy J. In-cylinder combustion visualization in an auto-igniting gasoline engine using fuel tracer- and formaldehyde-LIF imaging. SAE Paper 2001-01-1924; 2001.

[39] Westbrook CK, Dryer FL. Prediction of laminar flame properties of methanol-air mixtures. Combust Flame 1980;37:171.

[40] Longfield JE, Walter WD. The Radical-sensitized decomposition of formaldehyde. J Am Chem Soc 1955;77:6098-103.

[41] Hidaka Y, Taniguchi T, Tanaka H, Kamesawa T, Inami K, Kawano H. Shock-tube study of CH_2O pyrolysis and oxidation. Combust Flame 1993;92:365.

[42] Westbrook CJ. Chemical kinetics of hydrocarbon ignition in practical combustion systems. Proc Combust Inst 2000;28:1563-77.

[43] Kuwahara K, Ando H. Role of heat accumulation by reaction loop initiated by H_2O_2

decomposition for thermal ignition. SAE Paper 2007-01-0908; 2007.

[44] Takatsuto R, Igarashi T, Iida N. Auto-ignition and combustion of DME and n-Butane/air mixtures in homogeneous charge compression ignition engine. in: Proceedings of the 4th International Symposium COMODIA 1998: 185-90.

[45] Kappel C, Luther K, Troe J. Shock wave study of the unimolecular dissociation of H2O2 in its falloff range and of its secondary reactions. Phys Chem Chem Phys 2002;4:4392–4398.

[46] Azimov U, Okuno M, Tsuboi K, Kawahara N, Tomita E. Multidimensional CFD simulation of syngas combustion in a micro-pilot-ignited dual-fuel engine using a constructed chemical kinetics mechanism. Int J Hydrogen Energy 2011:36:13793-13807.

[47] CD-Adapco Inc., DARS Basic 2.10; 2015.

[48] Curran HJ, Pitz WJ, Westbrook CK, Dagaut P, Boettner JC, Cathonnet M. A wide range modeling study of dimethyl ether oxidation. Int J Chem Kinet 1998;30:229-241.

[49] Fisher SL, Dryer FL, Curran HJ. The reaction kinetics of dimethyl ether: I: High-temperature pyrolysis and oxidation in flow reactors. Int J Chem Kinet 2000;32:713-740.

[50] Fisher SL, Dryer FL, Curran HJ. The reaction kinetics of dimethyl ether. II: Low-temperature oxidation in flow reactors. Int J Chem Kinet 2000;32:741-759.

[51] Ranzi E, Frassoldati A, Grana R, Cuoci A, Faravelli T, Kelley AP, Law CK. Hierarchical and comparative kinetic modeling of laminar flame speeds of hydrocarbon and oxygenated fuels. Prog Energy Combust Sci 2012;38:468-501.

LIST OF FIGURE CAPTIONS

Figure 1. Typical hydrocarbon fuel oxidation in HCCI engine

Figure 2. Schematics of a compression-expansion test engine.

Figure 3. Schematic diagram of light absorbance acquisition setup.

Figure 4. Time-resolved absorbance spectra and ROHR at different pressures and temperatures

Figure 5. Time-resolved HCHO and OH absorbance peaks versus the maximum rate of heat release.

Figure 6. Time-resolved absorbance at intake absolute pressure 50kPa. The crank angle degree shown for each increment is the one when ICCD was triggered. The data for each increment was obtained with the exposure duration for 11° CA.

Figure 7. Time-resolved absorbance at intake absolute pressure 60kPa. The crank angle degree shown for each increment is the one when ICCD was triggered. The data for each increment was obtained with the exposure duration for 11° CA.

Figure 8. Time-resolved absorbance at intake absolute pressure 85kPa. The crank angle degree shown for each increment is the one when ICCD was triggered. The data for each increment was obtained with the exposure duration for 11° CA.

Figure 9. HCHO and OH absorbances at fixed exposure start timing and duration for different combustion cycles.

Figure 10. HCHO and OH absorbance trends at different intake pressures

Figure 11. HCHO and OH average absorbance level of combustion cycles at 308nm, 316nm, 328nm, 340nm and 354nm.

Figure 12. Chemical kinetics study of DME combustion in RCM with argon. T_{in}=293K, P_{EC} = 100bar; (A) DME/O_2 = 0.153 and O_2/Ar = 0.097; (B) DME/O_2 = 0.310 and O_2/Ar = 0.061; (C) DME/O_2 = 0.512, O_2/Ar = 0.040.

Figure 13. Chemical kinetics study of DME combustion in RCM with argon and N_2. (A) Argon: T_{in}=450K, P_{EC} = 100bar; DME/O_2 = 0.153, O_2/Ar = 0.097; (B) Argon: T_{in}=450K, P_{EC} = 100bar; DME/O_2 = 0.512, O_2/Ar = 0.040; (C) N_2: T_{in}=450K, P_{EC} = 100bar; DME/O_2 = 0.153, O_2/Ar = 0.097; (D) N_2: T_{in}=450K, P_{EC} = 100bar; DME/O_2 = 0.512, O_2/Ar = 0.040.

Figure 14. Comparison of the effects of intake temperature and end-of-compression pressure on HCHO and OH formation during rapid compression combustion of DME with argon. T_{in}=293K, 303K, 313K and 323K; P_{EC} = 20bar, 50bar, 80bar and 100bar; Case 1: DME/O_2 = 0.153 and O_2/Ar = 0.097; Case 2: DME/O_2 =0.512; and O_2/Ar = 0.040.

Figure 15. Combustion cycles with different in-cylinder pressure oscillations and knock intensities. Start of exposure for absorbance measurement is at 20 and 15 deg. before TDC and knock intensity (KI) is 0.27 and 0.67, respectively.

Figure 16. Combustion cycles with different in-cylinder pressure oscillations and knock intensities. Start of exposure for absorbance measurement is at 10 and 5 deg. before TDC and knock intensity (KI) is 0.13 and 0.06, respectively.

Figure 17. Combustion cycles with different in-cylinder pressure oscillations and knock intensities. Start of exposure for absorbance measurement is at 3 deg. before TDC and at TDC and knock intensity (KI) is 0.68 and 0.54, respectively.

Figure 18. Combustion cycles with different in-cylinder pressure oscillations and knock intensities. Start of exposure for absorbance measurement is at 2 and 5 deg. after TDC and knock intensity (KI) is 0.35 and 0.78, respectively.

Figure 19. Combustion cycles with different in-cylinder pressure oscillations and knock intensities. Start of exposure for absorbance measurement is at 10 and 15 deg. after TDC and knock intensity (KI) is 1.19 and 0.53, respectively.

LIST OF TABLE CAPTIONS

Table 1. Engine specification and initial conditions of fuel mixture for absorption experiment

Table 2. Initial mass fractions for chemical kinetics analysis

Table 1

Bore	78 mm
Stroke	85 mm
Connecting rod length	153 mm
Displacement volume	406.2 cm3
Compression ratio	9.0:1
Combustion chamber	Pancake type
Engine speed	600 rpm
Valve closure time	180 deg.BTDC
Equivalence ratio	0.3
Intake temperature	293K, 295K, 303K
Intake pressure	48kPa ÷ 85kPa

Table 2

	DME-O_2-Ar / DME-O_2-N_2		
	DME	O_2	Ar or N_2
Case 1 (A)	0.013406	0.087307	0.899287
Case 2 (B)	0.017232	0.056113	0.926655
Case 3 (C)	0.019453	0.038007	0.94254

Figure 1

Click here to download high resolution image

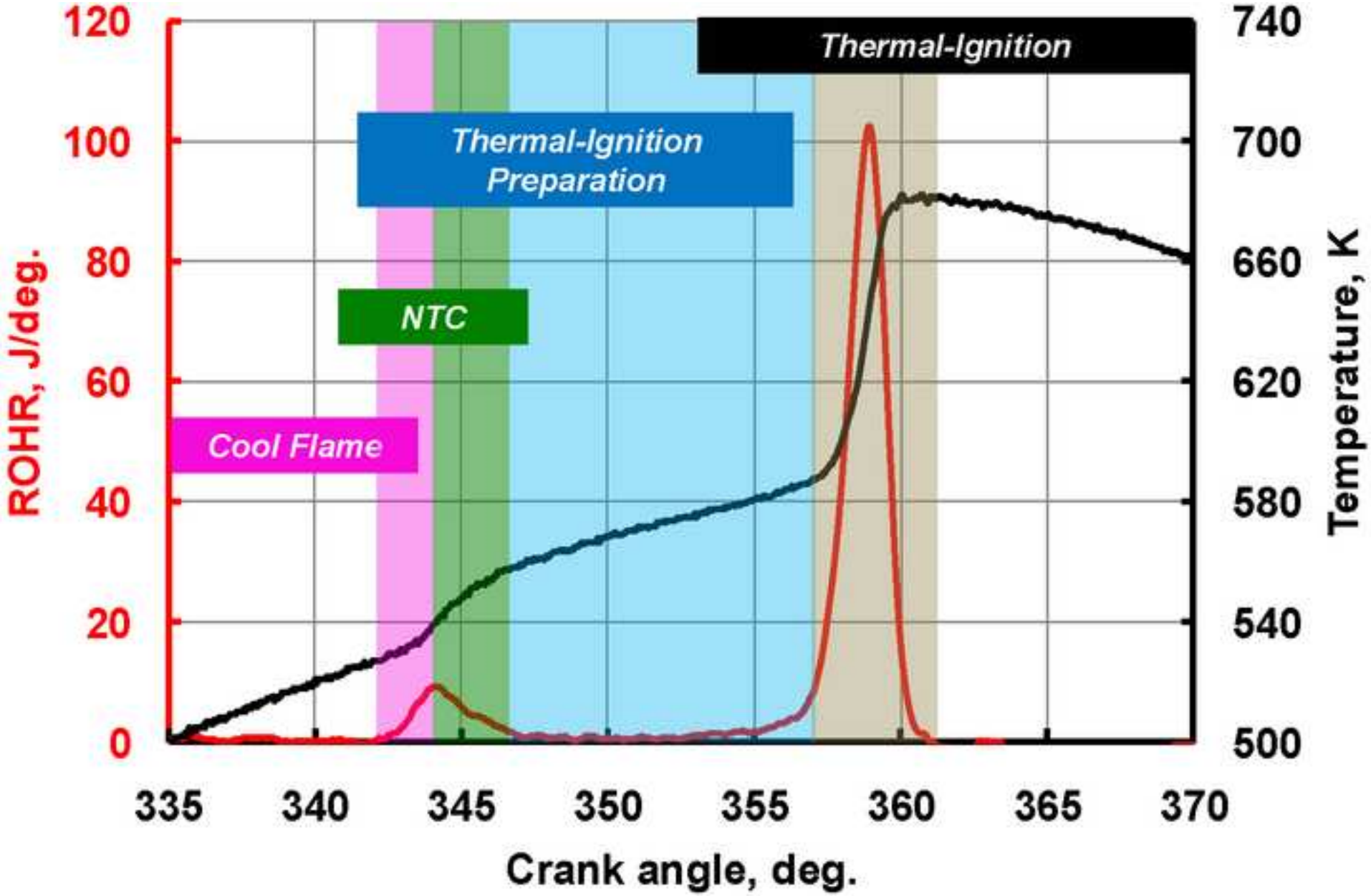

Figure 2

Click here to download high resolution image

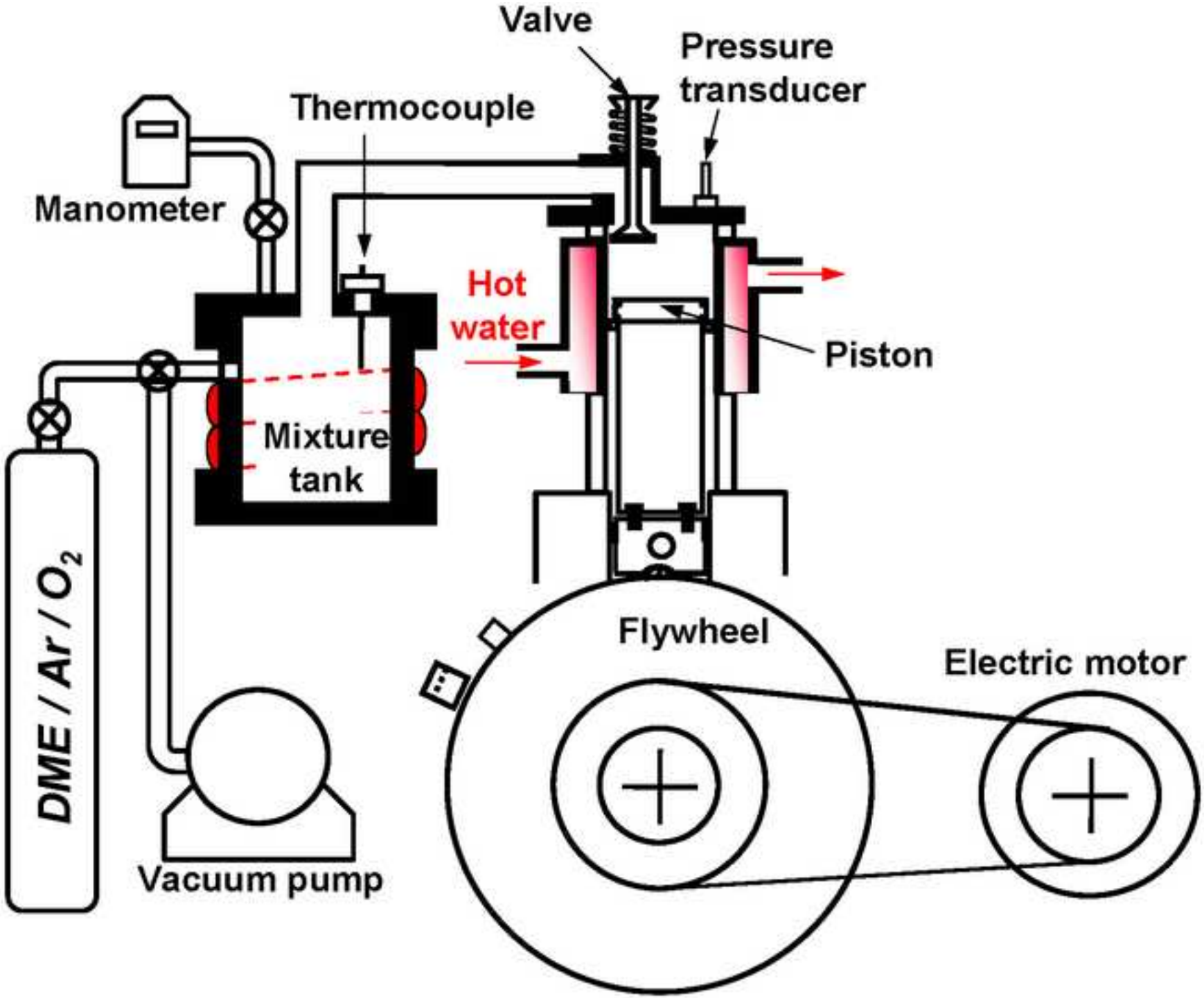

Figure 3

Click here to download high resolution image

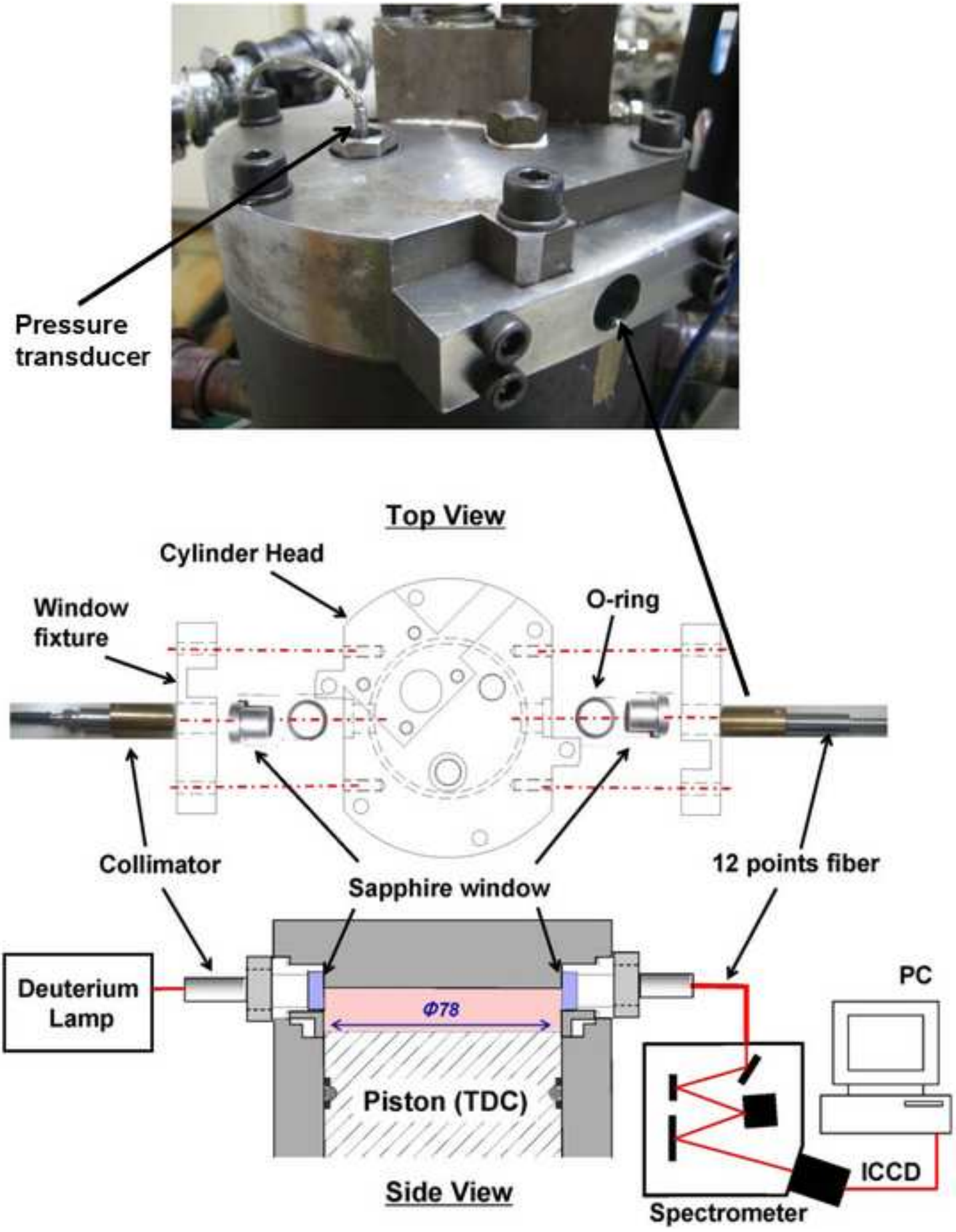

Figure 4

Click here to download high resolution image

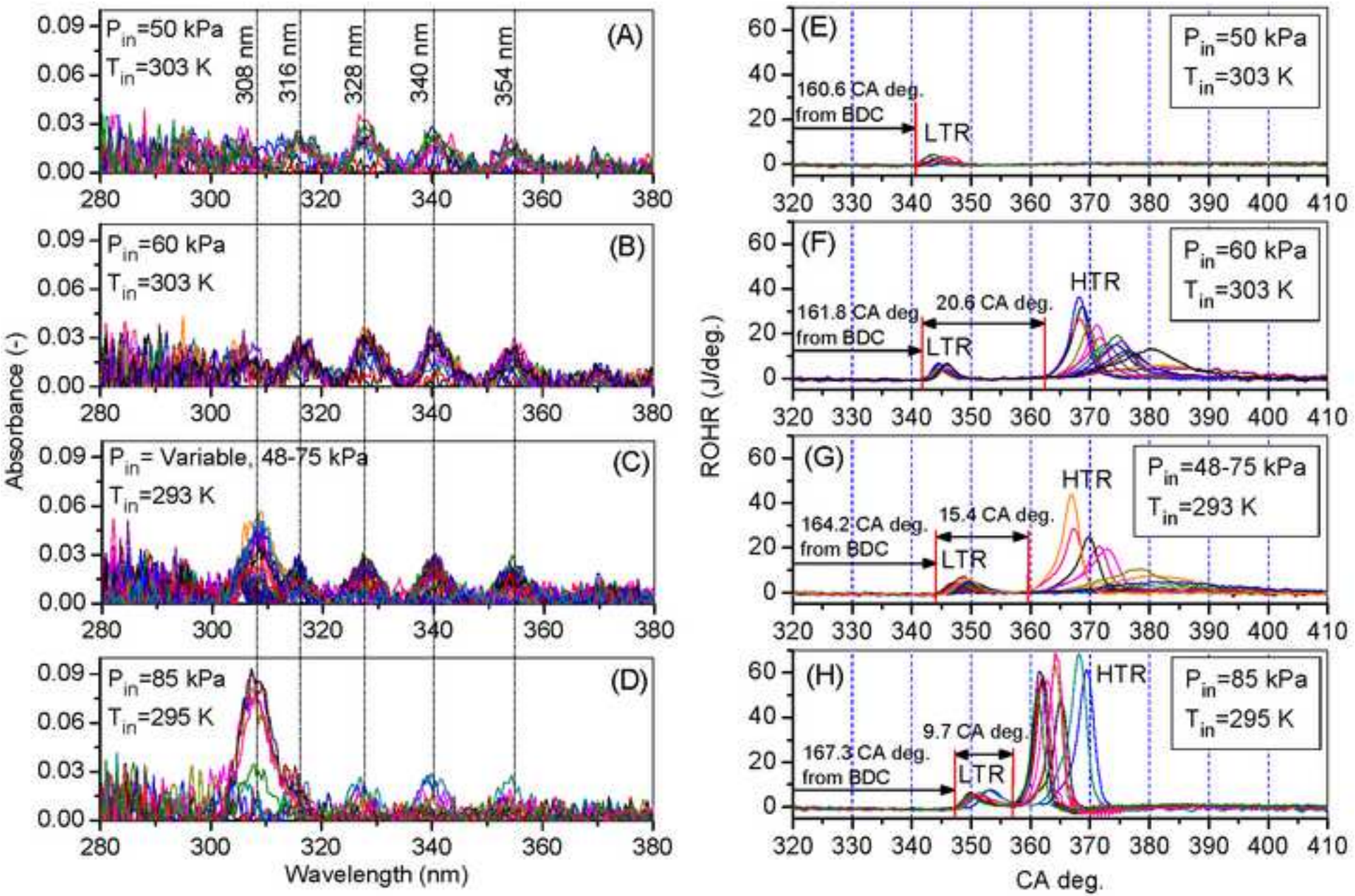

Figure 5

Click here to download high resolution image

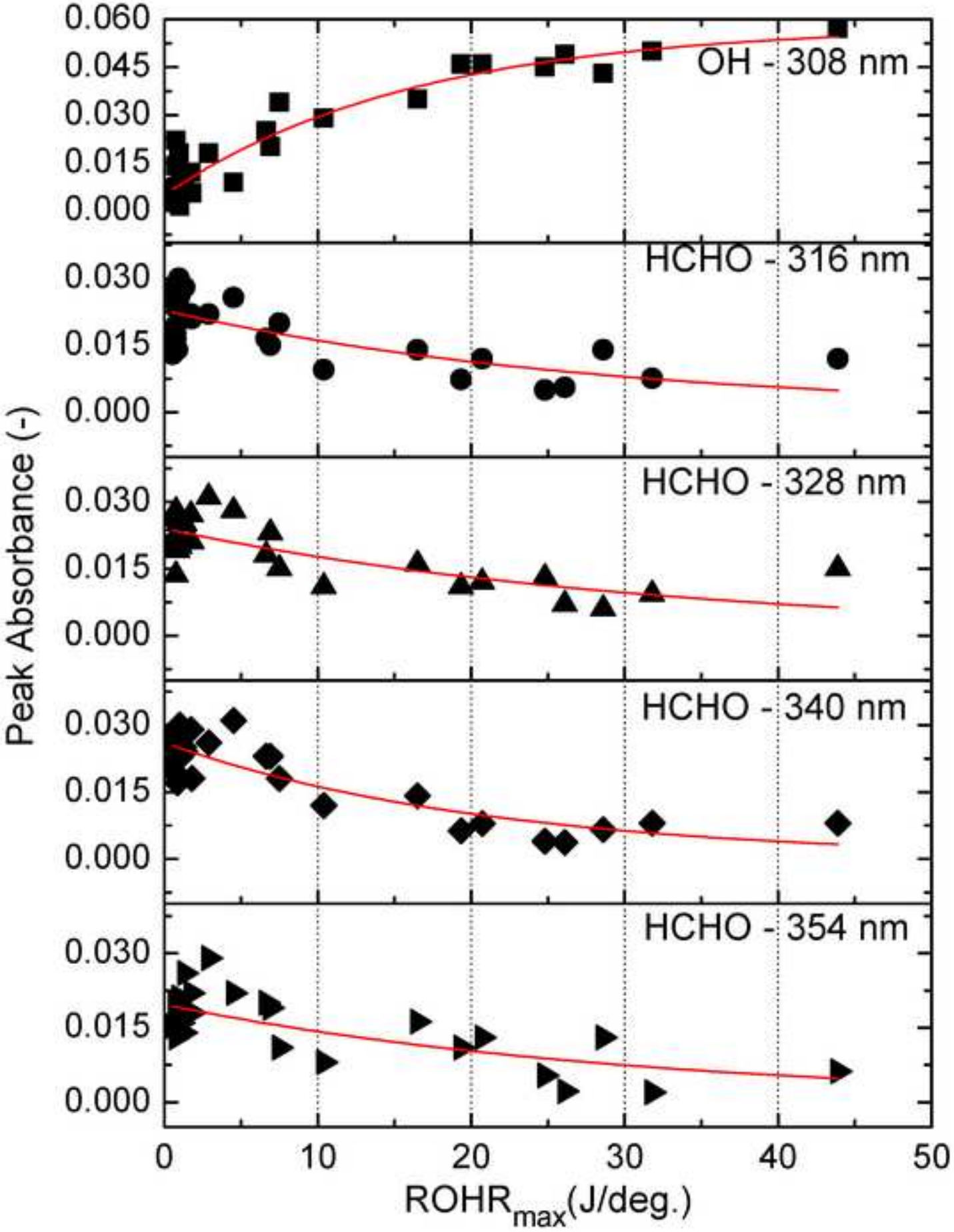

Figure 6

Click here to download high resolution image

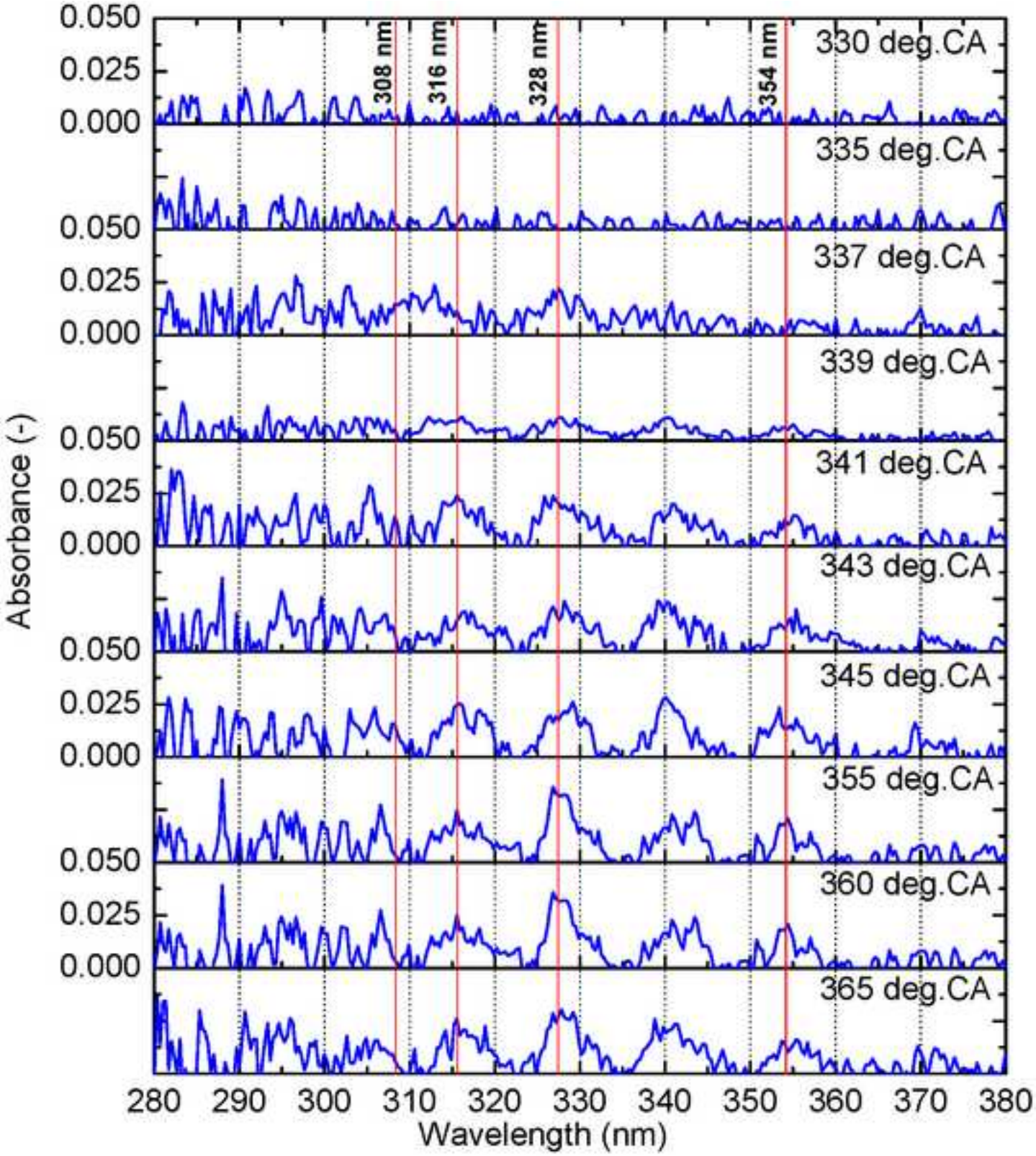

Figure 7

Click here to download high resolution image

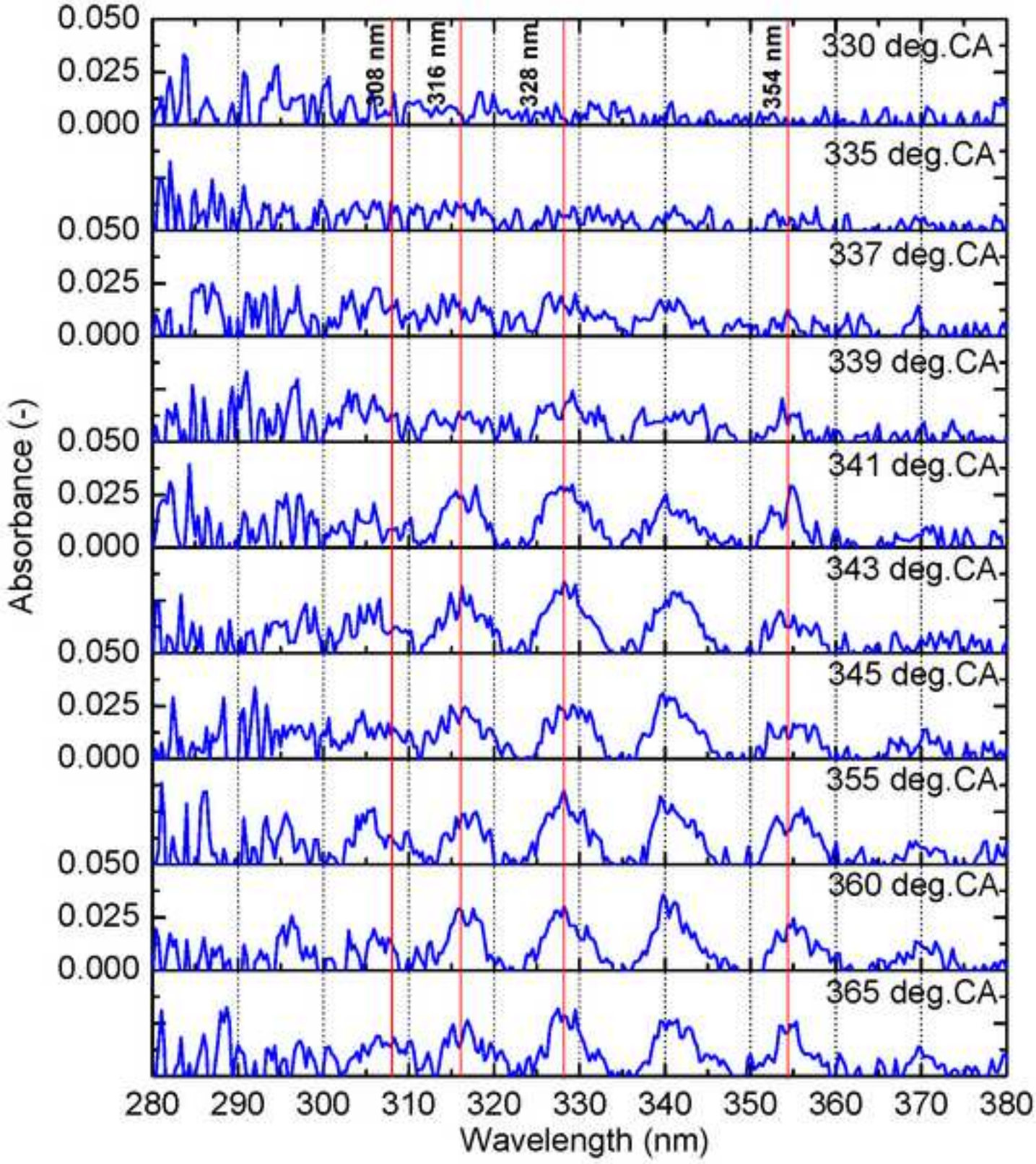

Figure 8

Click here to download high resolution image

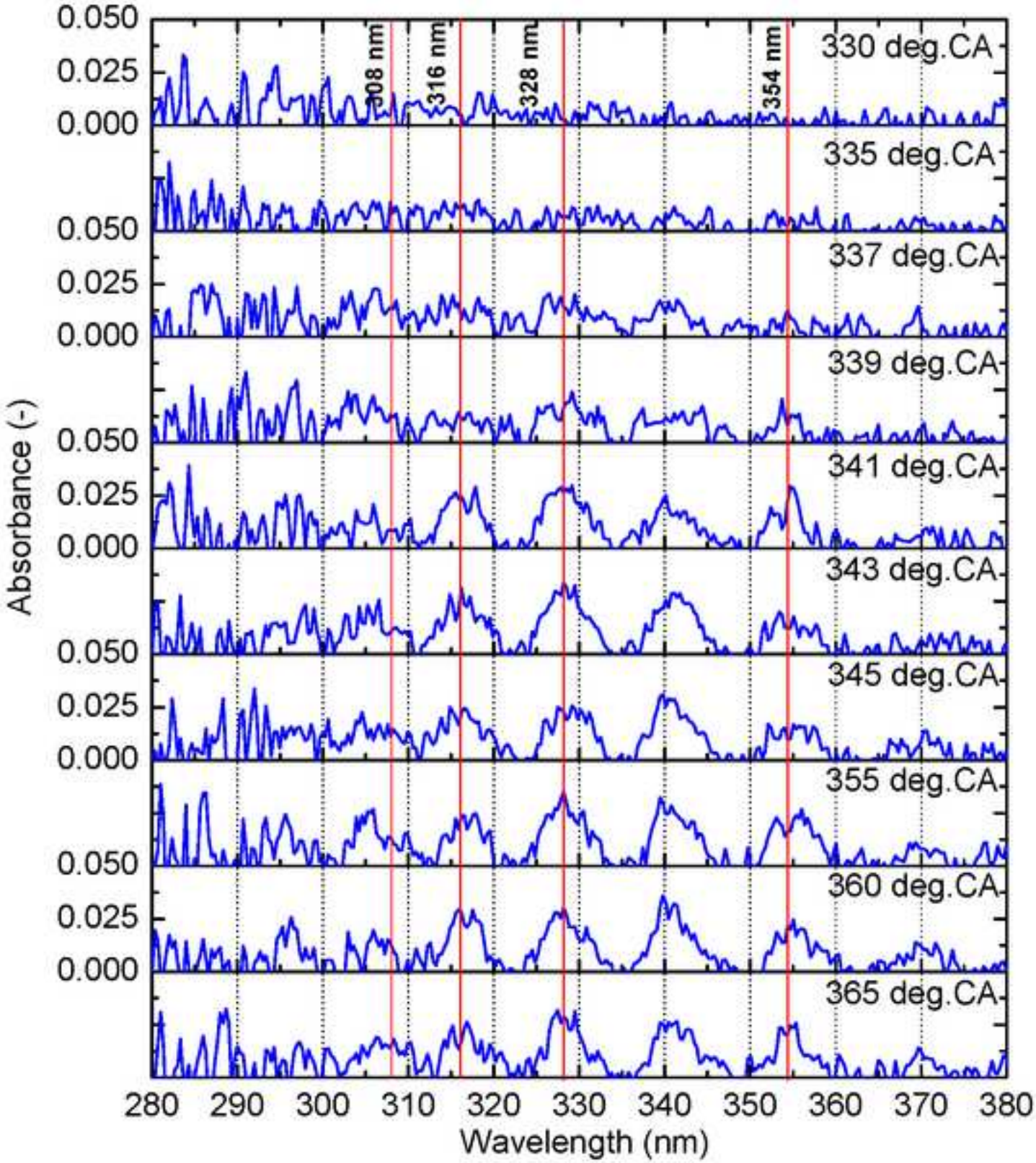

Figure 9

Click here to download high resolution image

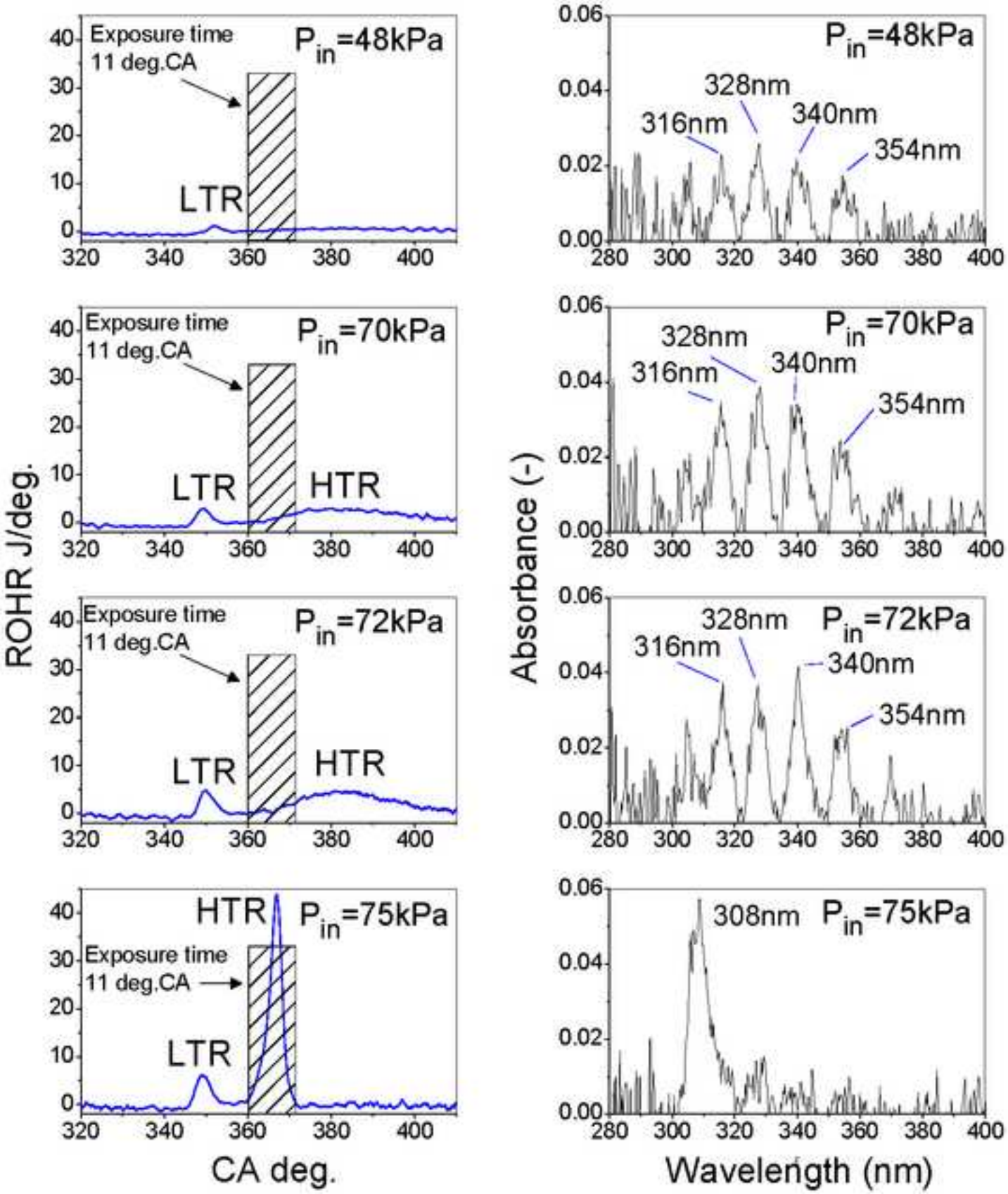

Figure 10

Click here to download high resolution image

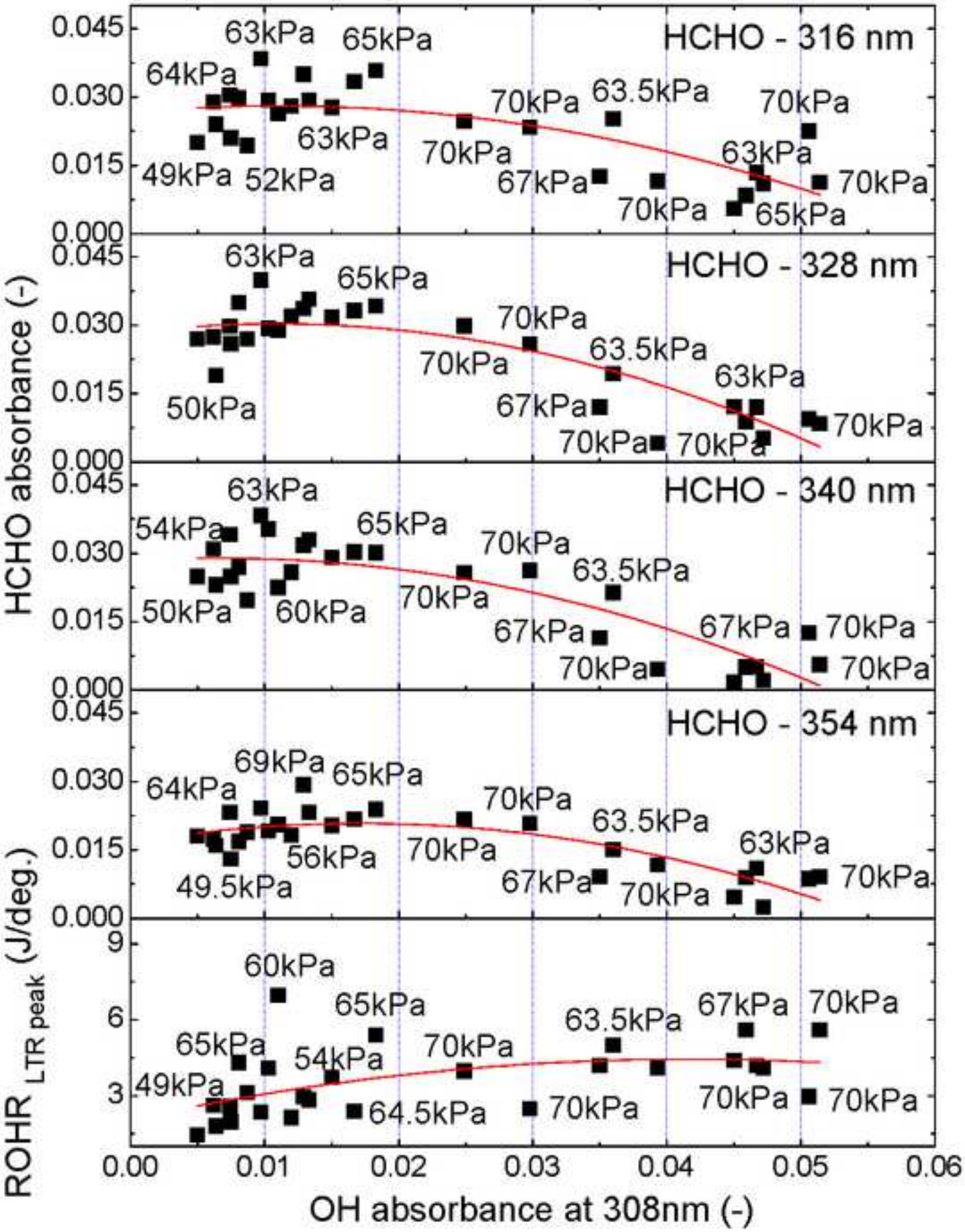

Figure 11
Click here to download high resolution image

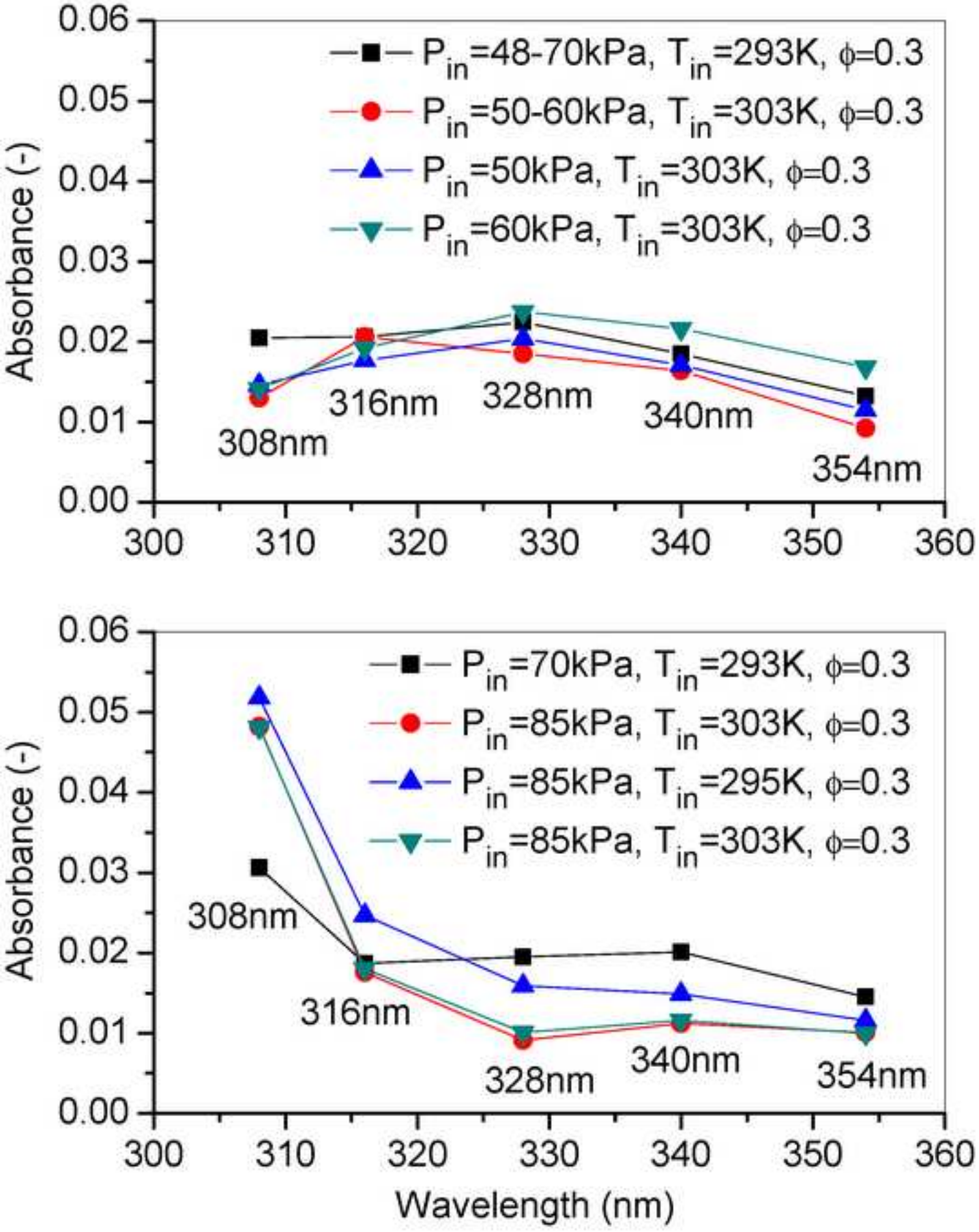

Figure 12

Click here to download high resolution image

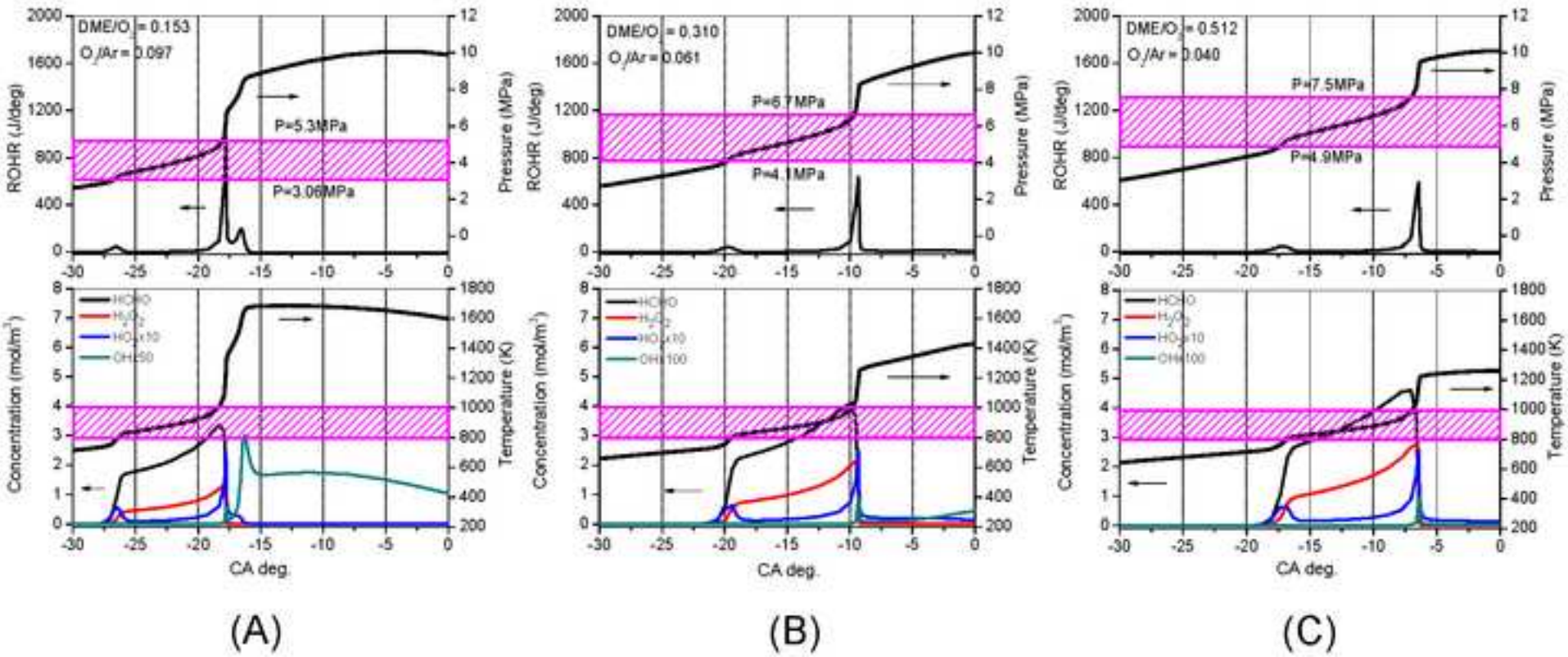

Figure 13

Click here to download high resolution image

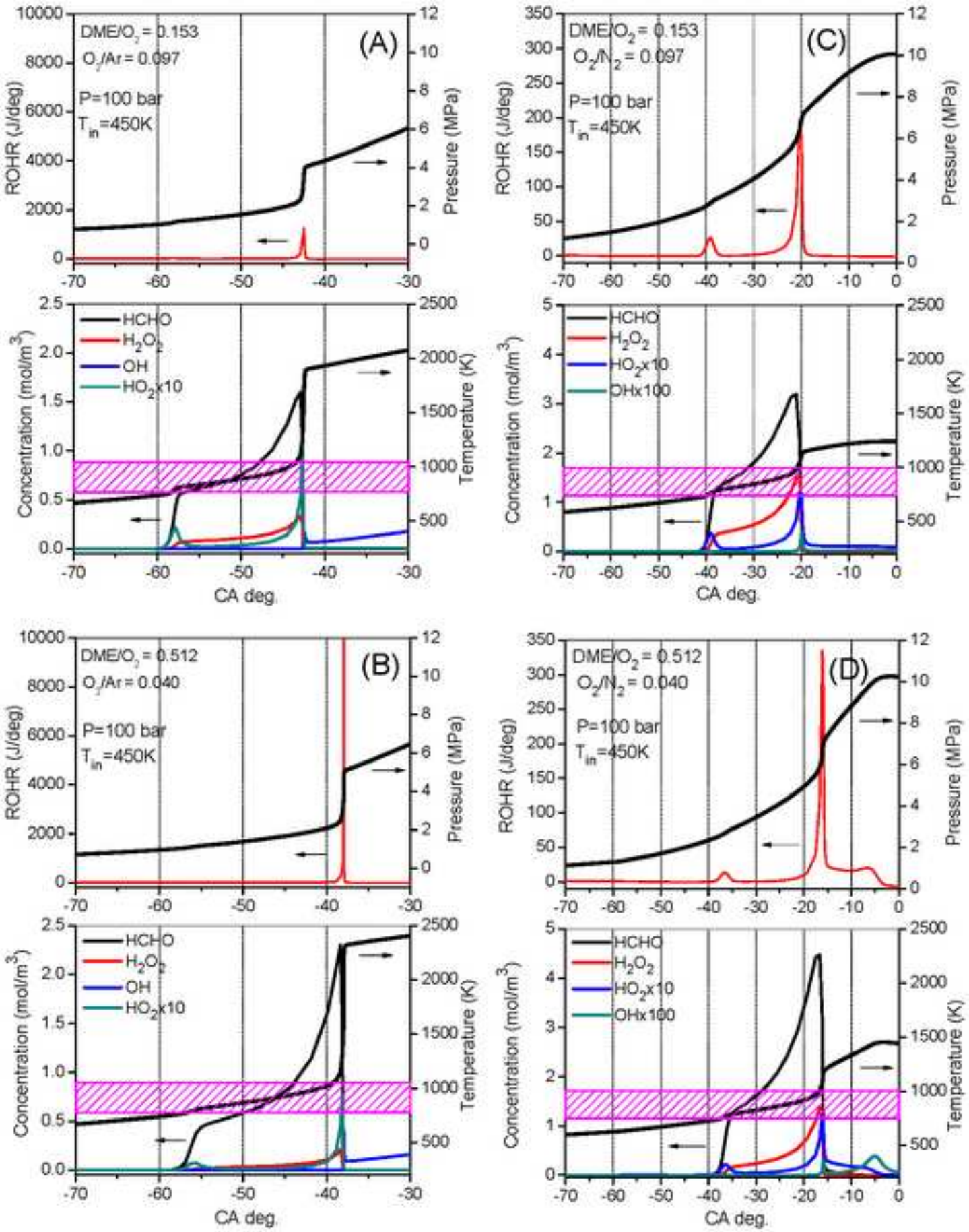

Figure 14

Click here to download high resolution image

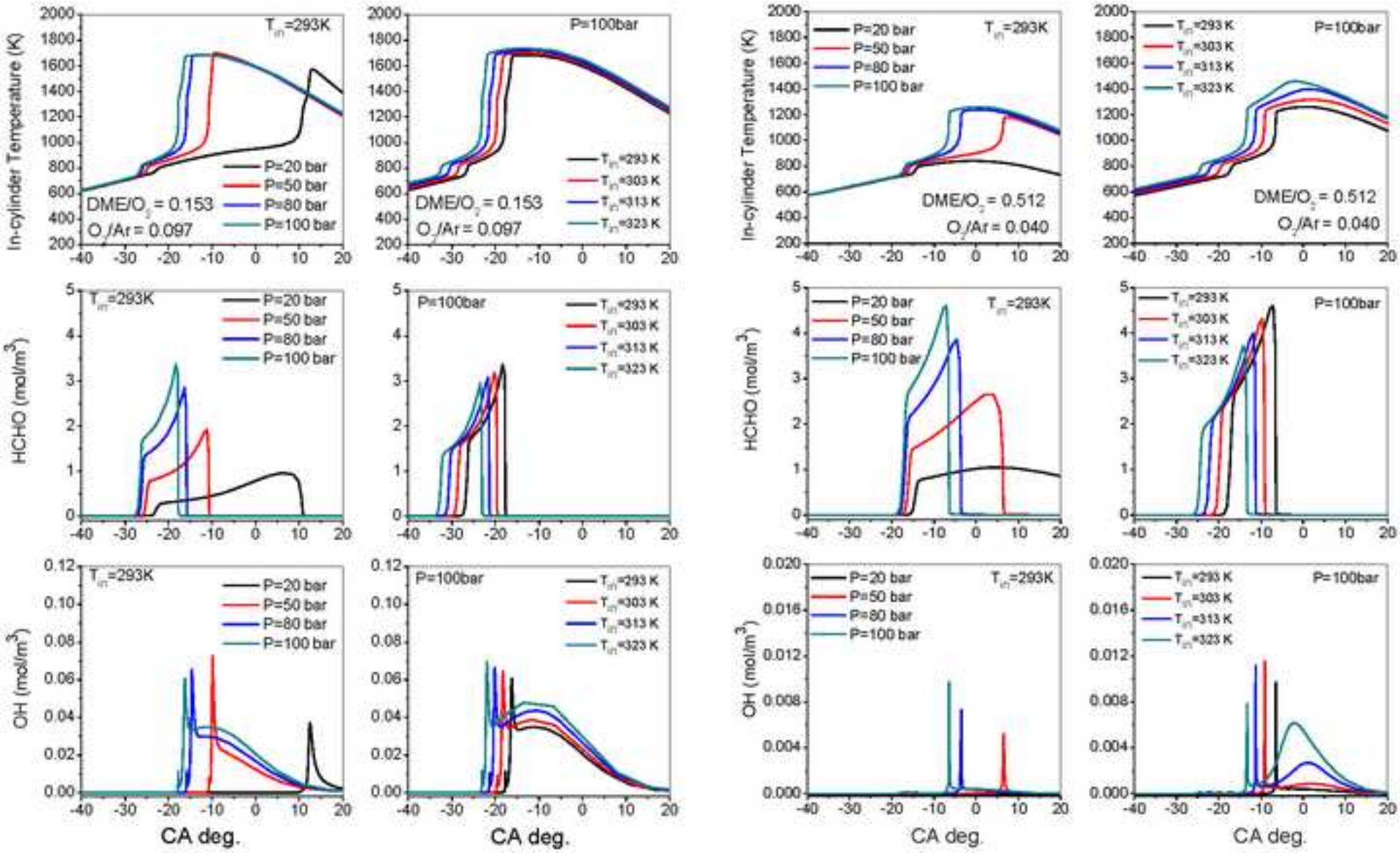

Figure 15

Click here to download high resolution image

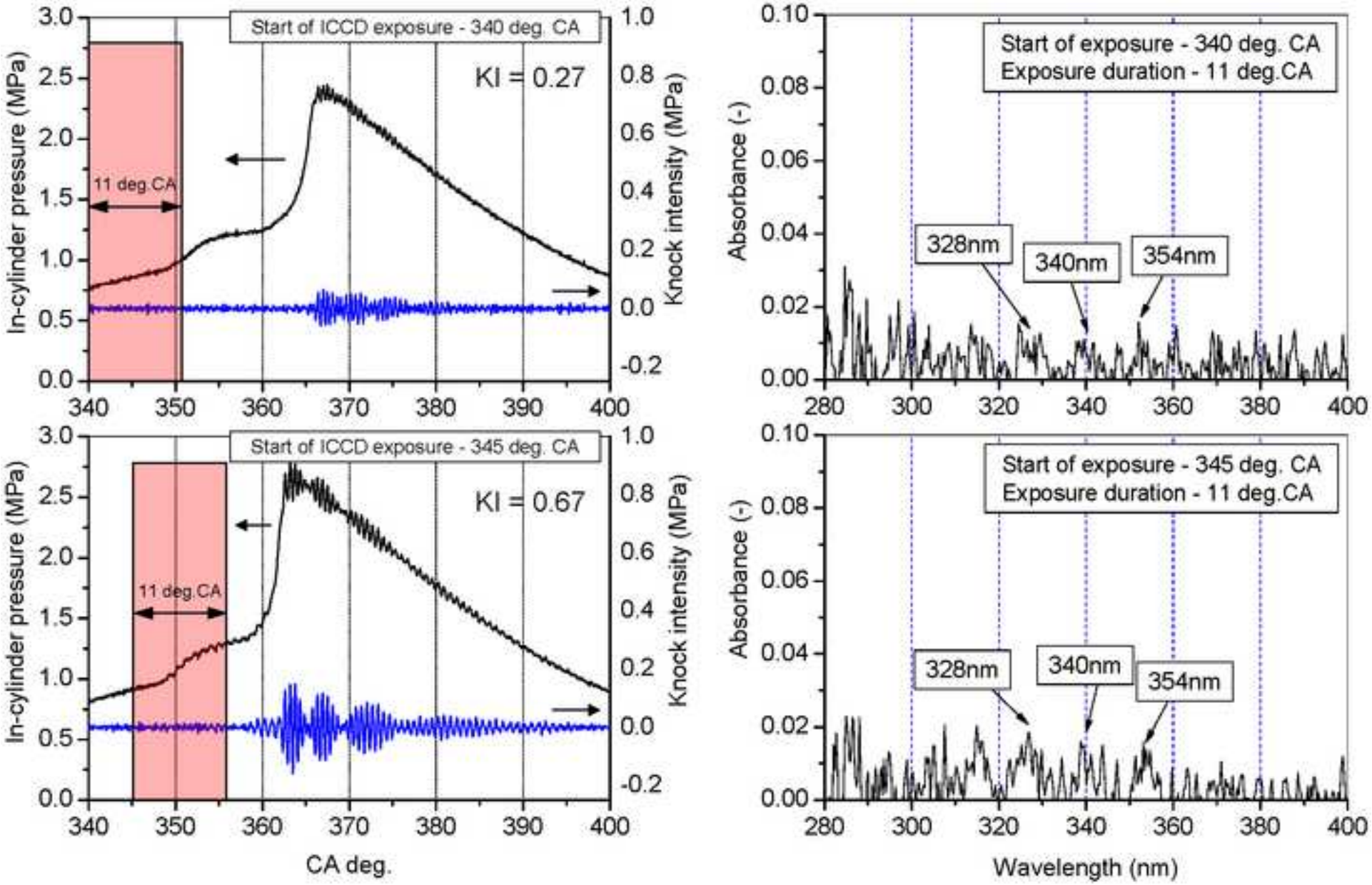

Figure 16

Click here to download high resolution image

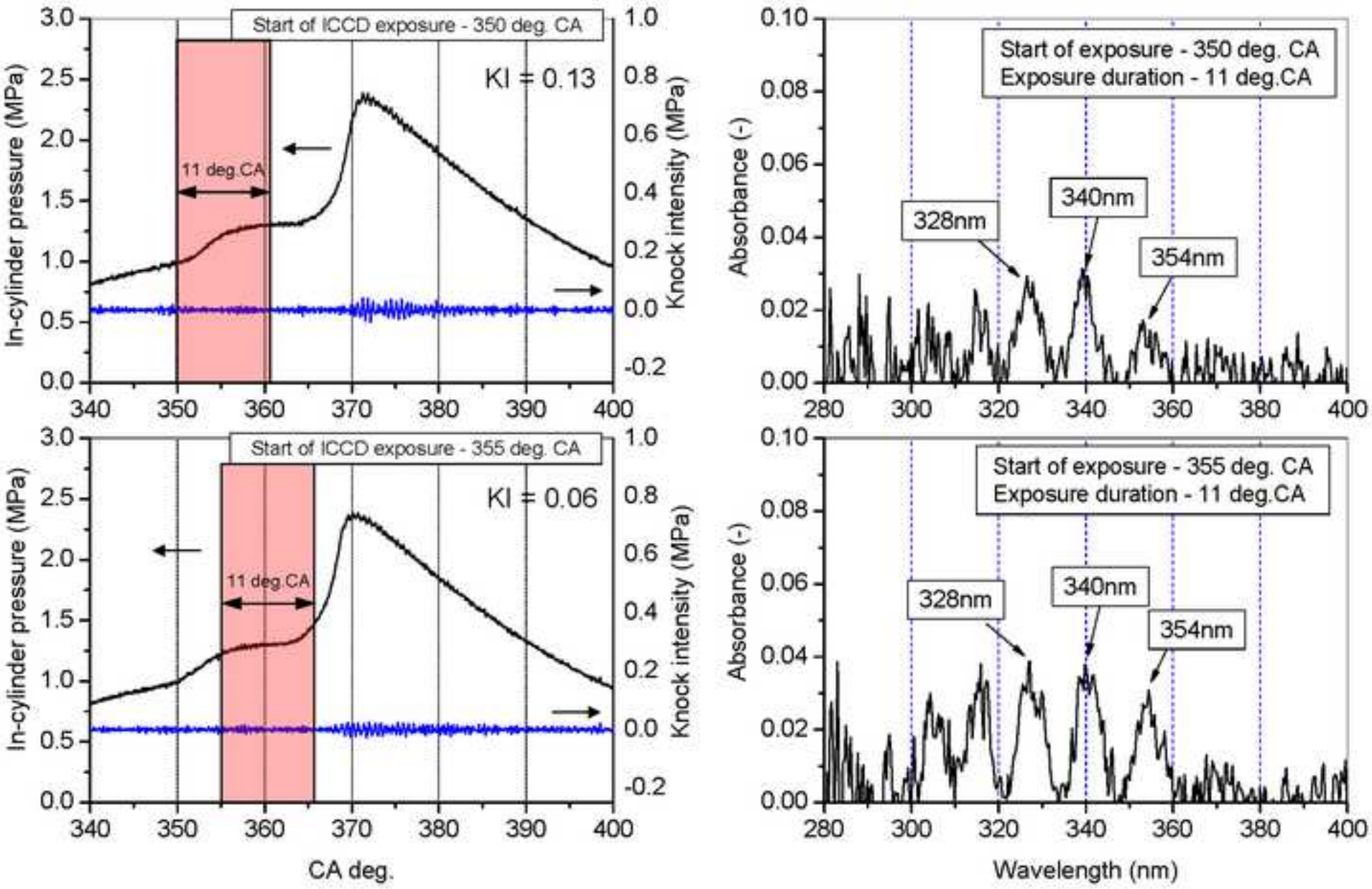

Figure 17

Click here to download high resolution image

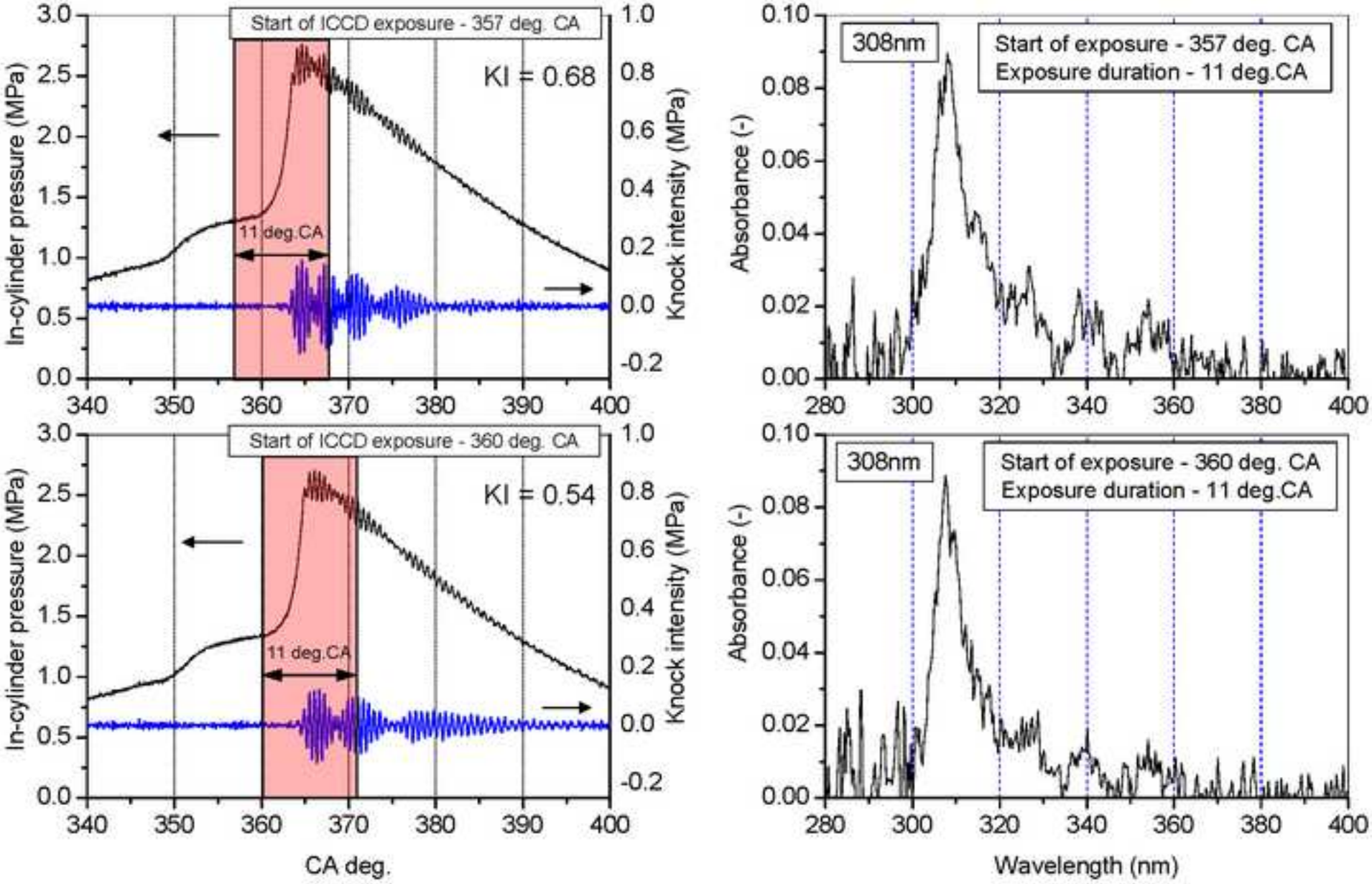

Figure 18

Click here to download high resolution image

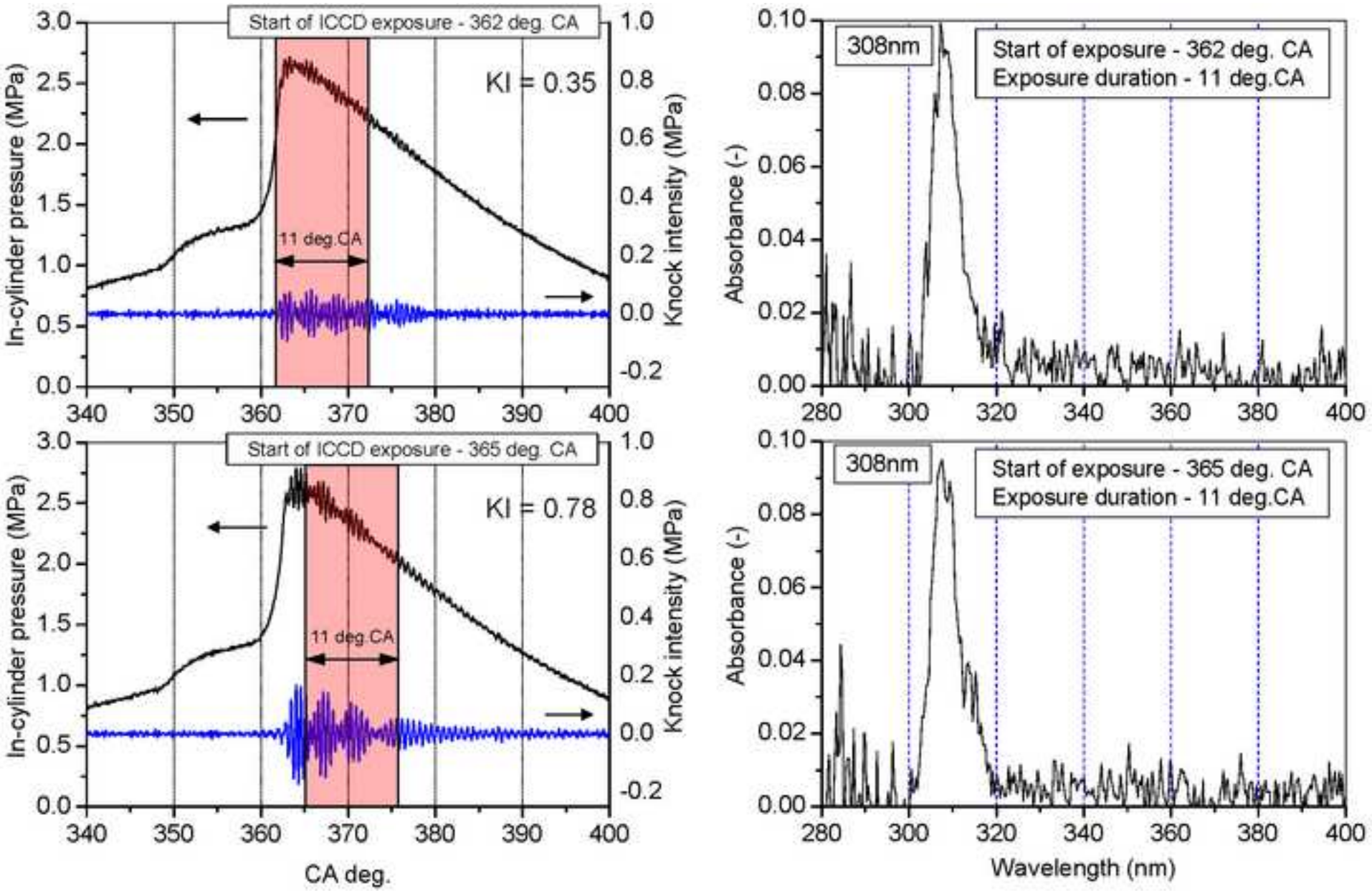

Figure 19

Click here to download high resolution image